Dust Particle Settling in Protoplanetary Disks around Young Stars in Binary or Multiple Systems

佐藤，康子

(Degree)
博士（理学）

(Date of Degree)
1998-03-31

(Date of Publication)
2009-05-12

(Resource Type)
doctoral thesis

(Report Number)
甲1768

(JaLCDOI)
https://doi.org/10.11501/3141090

(URL)
https://hdl.handle.net/20.500.14094/D1001768

博士論文

Dust Particle Settling in Protoplanetary Disks around Young Stars in Binary or Multiple Systems

(連星系・多重星系をなす若い星周辺の原始惑星系円盤におけるダスト粒子の沈澱)

平成10年1月

神戸大学大学院自然科学研究科

佐藤　康子

Contents

1 Introduction **3**

2 Evolution and structure of passive disks **8**

2.1 Classification of stars and disks 8

2.2 Structure of passive disks 13

2.3 Height of the absorbing surface 16

2.4 Dust particle settling 18

3 Protoplanetary disks around single young stars **22**

3.1 Model calculations 22

3.2 Sample single stars 25

3.3 Results with sample single stars 28

3.4 Verification of the standard model 30

4 Disks around young binaries or multiples **36**

4.1 Basic assumptions 36

4.2 Sample stars in binaries or multiples 37

4.3 Results with sample stars 38

4.4 Discussion 40

5 Conclusions and discussions **48**

Abstract

The main purpose of this paper is to report the results of a study to investigate dust particle settling in disks around young stars in binary or multiple systems. Recent IRAM observations provide us with the evidences of many candidates of protoplanetary disks around pre-main sequence stars. Using the observational data, we made a verification of our *passive disk model* which gives the radiation spectra from these young stars. We also mentioned the disk structure and dust particle settling in the disks around young stars in binary or multiple systems.

First, we describe the standard model of solar system formation and history of studies in this field from both theoretical and observational points of view. Our passive disk model is constructed on the basis of this standard model. We explain important processes of disk evolution which are reflected on observations. Among these processes dust particle settling towards the disk's midplane has a significant effect on the observed fluxes, especially. The height of the absorbing surface of central stellar radiation is altered by dust sedimentation, and it affects emergent luminosities from the disk.

Second, we review our passive disk model in detail. Here we adopt the nominal surface density of circumstellar disk. The radial temperature distributions of a disk is derived from balancing the thermal emission from the disk with the heating by the central stellar irradiation and by the turbulent motion inside the disk. In our calculation dust particle settling is taken into account by a f-factor, which represents the ratio of the absorbing surface height to gas scale height. Gas scale height can be treated as the height of absorbing surface of central star radiation in almost all the cases, but sedimentation of dust particles can alter this height.

Using this passive disk model, we performed model calculations and obtained the luminosity density from a typical young star which is presumed to have a circumstellar disk. We made a strong comparison of the result with each observed flux. Observed fluxes from many young stars are fitted well by our calcutaion and this assures the validity of our model. We find out many of these young stars are in binary or multiple systems from recent observations. From these observations, it is pointed out that binary separations have a correlation with the rate of disk formation. We investigated the relation between separations and f-factor, i.e., settling degree of dust particles. Contrary to our prediction that a close companion inhibits dust particle settling, the result shows that there is no significant correlation between binary separations and f-factors.

1 Introduction

The standard model of solar system (Hayashi et al. 1985 [1]) gives the most consistent picture of our planetary system formation. This model starts from a protosun and a circumstellar disk-like nebula with a low mass of $\sim 0.02\ M_\odot$ consisting of gas and dust, where $M_\odot$ denotes the solar mass. We call this disk a *protoplanetary disk* or simply a *solar nebula* in the present thesis. The protoplanetary disk is considered to be a by-product of the protosun formed by the gravitational collapse of a core in an interstellar cloud. To reproduce the present solar chemical abundance, a mixed gas is consideded to be composed mainly of H_2 and He.

Dust particles are considered to be a mixture of rocky (silicate) and icy (H_2O, CO_2, and so on) materials. During accretional phase, there occurs vigorous turbulent motion in the disk. Owing to the large turbulent viscosity, the disk gas continues to accrete onto the central protosun. The protosun grows via accretion of the gas materials which directly falls from the interstellar cloud and also accrets through the protoplanetary disk. When the mass of the protosun reaches the present solar mass, the gas infall from the cloud is almost completed. At the same time, the gas accretion through the disk is also completed because turbulent motion in the disk becomes weak. During the turbulent phase, dust particles are perturbed by turbulent motion and sufficiently mixed with gas molecules in the disk. Rotating around the central star with almost Keplerian velocity, the gas molecules drift at the height where the vertical component of the central star gravity is balanced with the pressure gradient. On the other hand, because of their lack of pressure force, the dust particles settle towards the central plane of the disk after the turbulence decays. Most dust particles sink onto the midplane in $10^3 - 10^4$ years except for very fine ones. These dust grains collide with each other and grow by sticking to form a thin dust layer around the midplane.

As the settling proceeds, the dust layer becomes thinner and thinner with a considerable increase of density. If the thickness of the dust layer becomes sufficiently thin (for example, $\leq 10^{-5}$ of the disk at 1 AU from the Sun, Nakagawa, et al. 1986 [22])[1],

[1]Recent study pointed out that it takes too much time to form such a thin dust layer (Sekiya 1997 [3]).

the density of the dust layer reaches the Roche density ρ_R (Jeans 1929 [2])

$$\rho_R = 3.53 M_\odot / a^3, \tag{1}$$

where a represents the distance from the Sun. When the density exceeds the Roche density, the dust layer is expected to fragment into numerous planetary embryos, or so-called planetesimals, on account of gravitational instability. These planetesimals, whose sizes are estimated to be the order of kilometers at 1 AU, accumulate through the mutual gravitational collisions. When massive bodies are formed, the growth of these bodies is accelerated because their gravity attracts the surrounding gas and hence, gas drag is greatly increased.

Finally they grow to form terrestrial-type planets ($\sim 1\ M_\oplus$, where $M_\oplus$ denotes the mass of the Earth) and cores of Jovian-type planets or so-called giant planets ($\sim 10\ M_\oplus$). The growing protoplanet with mass $> 10^{26}$ g attracts the gas by its own gravity and is surrounded by a relatively dense gas. The mass of the primordial atmosphere increases with the growth of the protoplanet. In the case of a very massive protoplanet, the self-gravity of the atmosphere is no longer negligible and the atmosphere collapses onto the surface of the protoplanet because of its gravitational instability. This instability of the primordial atmosphere and the subsequent gas capture process lead to the formation of the present giant planets. The remnant gas in the disk is expected to escape at some stage after the formation of Jovian planet (because it no longer exists at present). The gas may be blown out by solar wind or removed by giant planet perturbation, but the mechanism of dissipation of the solar nebula is still not obvious unfortunately.

Although this scenario had been mainly constructed by Safronov (1969) [4] and Hayashi and his co-workers in Kyoto group from the 1970's to the early 1980's, it was in the late 1980's that evidences of protoplanetary disks in extra-solar systems were found by observation. Since it is difficult to detect the protoplanetary disks as extended images with a ground-based telescope, most researchers thought that observation of these disks could be performed in the distant future. Then, InfraRed Astronomical Sattelite (IRAS), which was launched in 1983, found many infrared point sources inside and around molecular clouds by almost all-sky survey.

Since a part of these sources are invisible in optical wavelengths and have quite low temperatures ($\sim$ 100 K), they are regarded as protostars shining by releasing gravitaional energy on dynamical accretion of gases. On the other hand, many of the objects which are also visible in optical wavelengths are identified as T Tauri stars. IRAS observed much stronger infrared emission from T Tauri stars than that expected by blackbody radiation of the surface temperature of these stars. These infrared excesses can be well explained by the assumption of a thin disk which contains dust particles and extends from the surface of the central star to some 100 AU.

Stimulated by the excellent results of IRAS, observations of young stars have been performed by various methods since then. With millimeter array at Nobeyama Space Radio Observatory of National Astronomical Observatory, Japanese group also detected the thermal emission from dust particles around T Tauri stars. Compared with dust particles, the efficiency of generating infrared emission by gas molecules is lower, and hence to detect gaseous materials is quite difficult even if they also exist in the disk. In 1992, with 45 m radio telescope and millimeter array at Nobeyama Radio Observatory, gas components of a possible protoplanetary disk around GG Tau was observed for the first time. This result strengthened the evidence of the existence of protoplanetary disks. The disk masses are estimated to be $\sim 0.1 - 0.01\ M_{\odot}$ from photometric observations at optically thin millimeter wavelengths (Adams, Emerson, & Fuller 1990 [5]; Beckwith et al. 1990 [23]). The disk sizes are also estimated to be $\sim$100 AU from the fitting of spectral energy distributions (SEDs) at infrared wavelengths (Adams, Lada, & Shu 1988 [6]). The parameters of such disks are consistent with the values predicted by the so-called standard model of minimum solar nebula.

In this study we obtain the temperature distributions and SEDs of thermal emission of protoplanetary disks using our passive disk model (the scenario of planetary system formation based on the standard model, which we will describe in chapter 2 concretely), and compare the theoretical SEDs with recent observations. From the comparison, it is shown that the particle settling predicted by our model really occurs in many observed protoplanetary disks.

The fundamentals of calculation we employed in this paper are as follows. We

consider that the radiation from the central star is absorbed not by gas molecules but by mainly dust particles in the disk. When particles begin to settle, the absorbing surface of the central stellar radiation becomes lower than the gaseous disk surface itself. As the absorbing surface becomes lower, the incident angle of the radiation from the central star gets shallower and hence, the heating ratio decreases. Taking this lowering effect of the absorbing surface into account, we calculate the radial temperature distribution, and also spectrum, of thermal emission of the disk associated with a representative T Tauri star as a model example.

Recent IRAM observations (Osterloh & Beckwith 1995 [7]) provide us with evidences of disk formation around young stars in Taurus-Auriga cloud complex. A wide variety of these young stars, such as Herbig AeBe stars [33] and FU Orionis [34] have been studied and the observational data have been accumulated. It is remarkable in particular, that many disk candidates have been detected around young stars in binary or multiple systems, whereas the standard model we described above deals with a single star and its circumstellar disk. It has been considered so far that in such binary or multiple systems circumstellar disks are hard to form or, even if such disks form, they will be soon destroyed by the gravitational perturbation from the companion star.

The above observation stimulated us to investigate the disk formation and dust particle settling in such systems. From the observations it is shown that the binary separation has an effect on particle emission from the two component stars, and that single stars are more likely to have strong emission than binaries. These results also hold, if members of multiple systems with more than two components are included in the samples. Applying the model calculation described in the above paragraph to each observed source, whose parameters (L_*, M_*, T_*, and so on) are well-known, we compared theoretical spectrum with observed luminosities from these stars. Observational data of most stars including binaries are well-fitted by our passive disk model. We examine the correlation between the binary separation and degree of dust particle settling. From the fitting, we can see the degree of dust particle settling, or disk flaring in each source. In spite of our expectation that a close binary separation will inhibit dust sedimentation, there is no significant correlation between the phenomena.

In chapter 2, we will review the disk structure based on our passive disk model. Assuming a sufficiently thin disk, we obtained the density and temperature distributions of passive disks. We will give the formulae of them and also mention the change of the heating ratio from the central star caused by settling of dust particles. In chapter 3, we will explain our SEDs calculation in detail and show the model calculation of the passive disk around a typical young star. Then we will show the results of SEDs calculation of each sample star and compare the results with recent observational fluxes. Not only disks around single stars but also disks around stars in binary or multiple systems are included in our samples. We will investigate the configuration of the disk and dust particle settling around young stars in binary or multiple systems and present our results. Conclusions and discussions are summarised in chapter 4. A detailed explanation for the formula deriving the temperature distribution of the disk is given in appendices.

Figure 1: Distribution of T Tauri stars in H-R diagram: T Tauri stars are plotted with open circles. Each solid curve represents the evolution track of the star with the denoted mass. Main sequence stars are distributed in the gray belt region.

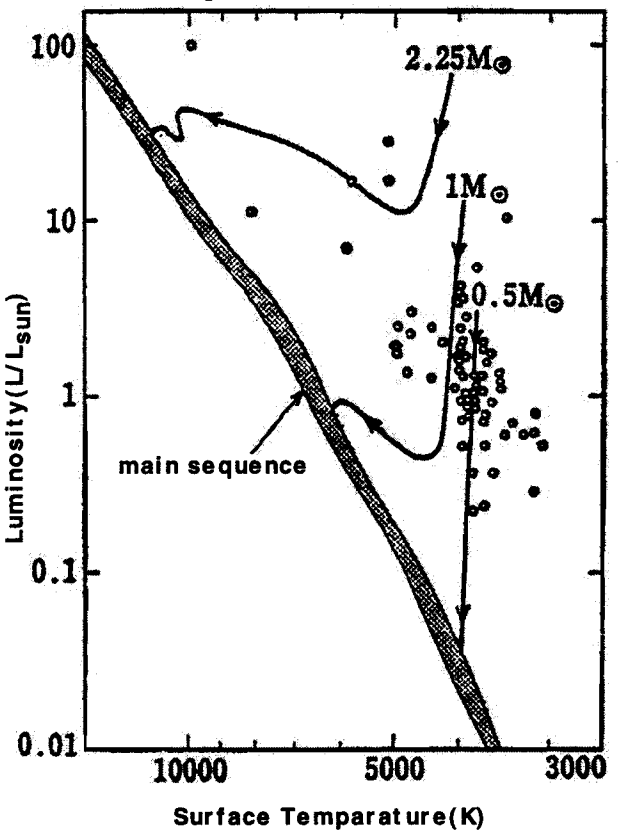

2 Evolution and structure of passive disks

2.1 Classification of stars and disks

CTTSs and WTTSs

Many stars which are considered to have protoplanetary disks are young variable stars called T Tauri stars (T-type stars in Taurus). T Tauri stars are located right above the main-sequence belt in the H-R diagram (Fig. 1). This means T Tauri stars have higher luminosities and lower surface temperatures than main sequence stars (stars shining by hydrogen burning in the central region). T Tauri stars are regarded as being in the transition phase of the evolution towards the main-sequences and contract

quasi-statically releasing the internal thermal energy. In this phase hydrogen burning in the central region of the star has not started yet. The lifetime of T Tauri stars is considered to be the order of $10^6 - 10^7$ yrs. On account of their rapid evolution, however, it is quite difficult to estimate the accurate age of each T Tauri star from the position in H-R diagram.

Figure 2: Spectrum of typical CTTS and WTTS

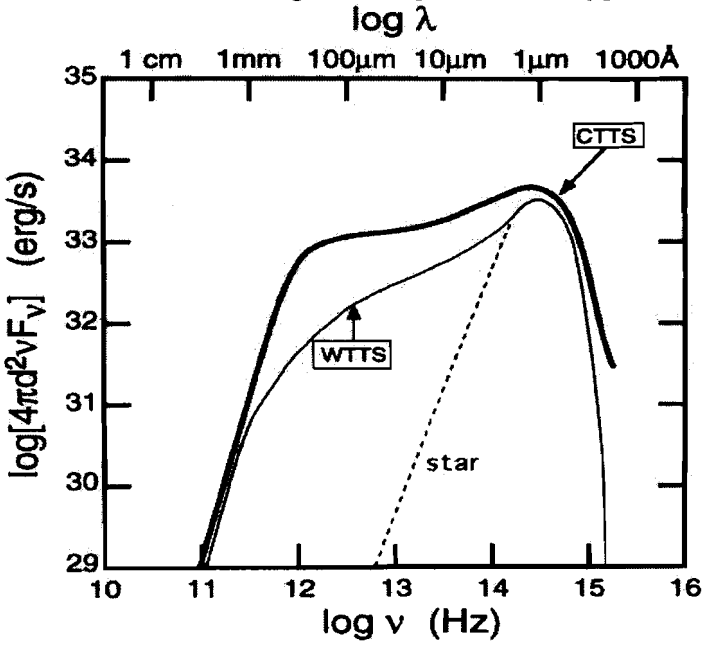

From an observational point of view, T Tauri stars are classified into two most important stellar types: classical T Tauri stars (CTTSs) and weak-line T Tauri stars (WTTSs). The majority of T Tauri stars which were previously observed are assigned to CTTSs with strong emission lines. Nearly half of the stars have detectable emission which has been attributed to thermal radiation from small particles contained in circumstellar disks. On the other hand, a new class of stars called WTTSs were found by X-ray observations of Einstein Sattelite which was launched in 1978. WTTSs have weaker emission lines compared to CTTSs. Thus, in order to distinguish previouly observed T Tauri stars from WTTSs, they were called "classical" T Tauri stars.

CTTSs are defined by $ew(\mathrm{H}\alpha) \geq 10$ Å, where $ew(\mathrm{H}\alpha)$ is the equivalent width of $\mathrm{H}\alpha$ emission lines, and WTTSs are their weaker counterparts. The origin of the $\mathrm{H}\alpha$

emission line remains uncertain and, therefore, the physical meaning of the distinction between CTTS and WTTS is somewhat unclear. Provided that the broadened emission lines were due to the thermal broadening, the width 10 Å would correspond to the temperature $\sim 3\times10^6$ K (order of coronal temperature) and can be regarded as a degree of some activities around the star. Although the detailed process of formation of Hα emission is still unknown, the most plausible interpretation is that these lines arise from some activities in the boundary layer between the central star and circumstellar disk. Many astrophysicists consider that CTTSs evolve into WTTSs, which seems correct in almost all cases, but there exist some CTTSs older than WTTSs. The ages of T Tauri stars have been estimated from their positions in the H-R diagram and seem to include some uncertainty. This uncertainty is attributable to two main reasons. First, it is difficult to separate stellar contribution from total luminosity. Second, the standard theory of pre-main-sequence evolution may be altered appreciably owing to mass accretion through the disks. (Thus, the classification of T Tauri stars according to central stellar ages may be inappropriate.)

Figure 2 shows typical examples of radiation spectra of these T Tauri stars. Luminosity densities L_ν ($L_\nu = 4\pi D^2 \nu F_\nu$, where D, ν and F_ν denote the distance from the star, frequencies, and observed fluxes, respectively) are plotted against frequencies in logarithmic scale. The broken line represents the blackbody radiation from a typical young star accompanied by no disk. The bold and fine solid curves correspond to the spectrum of CTTS and WTTS, respectively. In CTTSs large excesses of radiation spectrum can be seen in almost all region of infrared wavelengths as compared with the common young stars. This is considered to be due to the existence of a circumstellar disk having intrinsic heat source in itself. We can see WTTSs exhibit significantly less emission than CTTSs especially from near- to mid- infrared wavelengths. This means the inner part of the disk with higher temperatures, which is closer to the central star, is invisible. This is attributed to the decrease of the mass and temperature of the disk, but the details are still not clarified. Possible interpretations are as follows. Disk materials of the inner part has already fallen to the central star. Macroscopic objects such as planetesimals has been formed in the inner region.

Active and passive disks

Protoplanetary disks are also divided into two main categories from observation. We will denote central stellar luminosity with L_* and disk luminosity with L_d, hereafter. Disks having higher luminosities than the central stars (i.e. $L_d \gtrsim L_*$) are called active disks, and those with lower ones passive disks. As we will describe later, the former is considered to be in the early stages of the disk evolution and the latter in the late stages. Figures 3 and 4 give schematic views of active and passive disks, respectively. In Fig. 3 accretion of disk materials towards the central star is represented by arrows. Spring-like curves in the disk represent turbulent motions. Many dots depicted in the disk correspond to dust particles. By contrast, in passive disks turbulent motion due to mass accretion in the disk has already ceased and therefore no turbulence is illustrated in Fig. 4. Possible heat source of the disk becomes irradiation by the central star in this phase. Both of these Figures represent flaring disks in which settling of dust particles has not started yet. The passive disk, however, include various disks in different stages of dust particle settling.

Protoplanetary disks are formed by the gravitational contraction of cores of a molecular cloud. Immediately after the beginning of contraction, gas molecules surrounding the central star accrete on the stellar surface. After that, gas molecules with large angular momentum fall down onto the stellar surface to form a disk. In this stage the disk mass is still not very large and the central star corresponds to a *protostar* observationally. As the disk mass increases with subsequent accretion of gaseous materials, turbulent motion inside the disk becomes violent due to the self-gravitational instability of the disk. This leads to the enhancement of mass accretion rate $\dot{M}$ and efficient growth of the central star. In this *active disk* phase the central star is considered to be the *CTTS* observationally. Before long the gas accretion from cores of the molecular cloud ceases for some reason, and the disk mass decreases and the disk is stabilized against the self-gravitational instability. Then the turbulence is weakened and mass accretion rate $\dot{M}$ decreases. Planet formation becomes possible in this *passive disk* phase and the central star of this phase corresponds to *WTTS* observationally. Although the

correspondence of CTTSs to active disks and WTTSs to passive disks does not always hold, it is correct in most cases.

Figure 3: Active disk

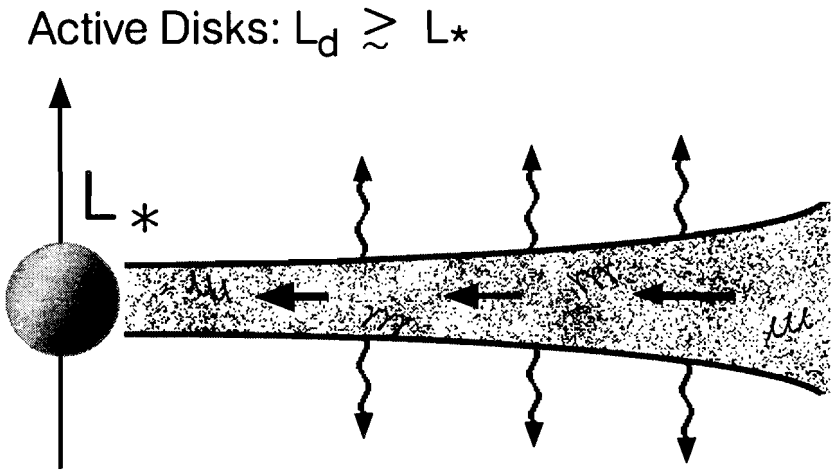

Figure 4: Passive disk

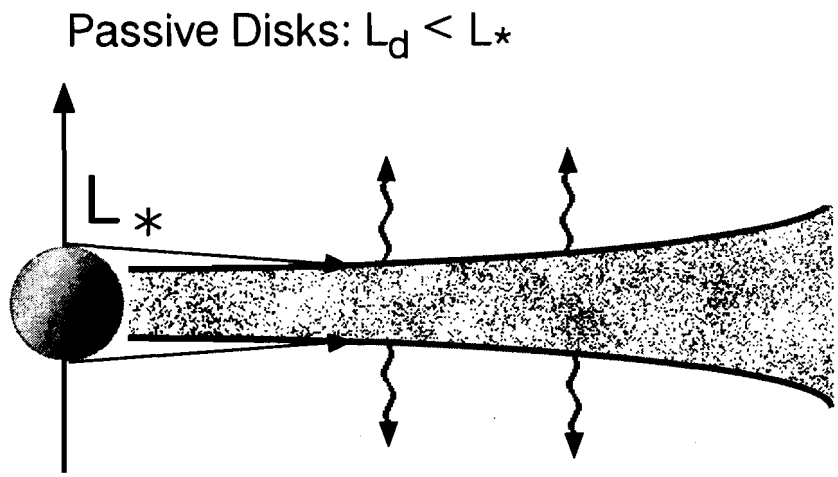

2.2 Structure of passive disks

In this section, we will discuss theoretical models for the structure of passive disks around T Tauri stars. We assume that the disks are optically thick for the stellar light ($\lambda \sim 1$ μm) and extends from the surface of the central star to 100 AU. In the folowing discussion we use the cylindrical coordinate (r, ϕ, z) centered on the central star and the midplane of the disk is assumed to be present on the plane $z = 0$ (Fig. 5). Axisymmetry is assumed with respect to z-axis.

Figure 5: Cylindrical coordinate

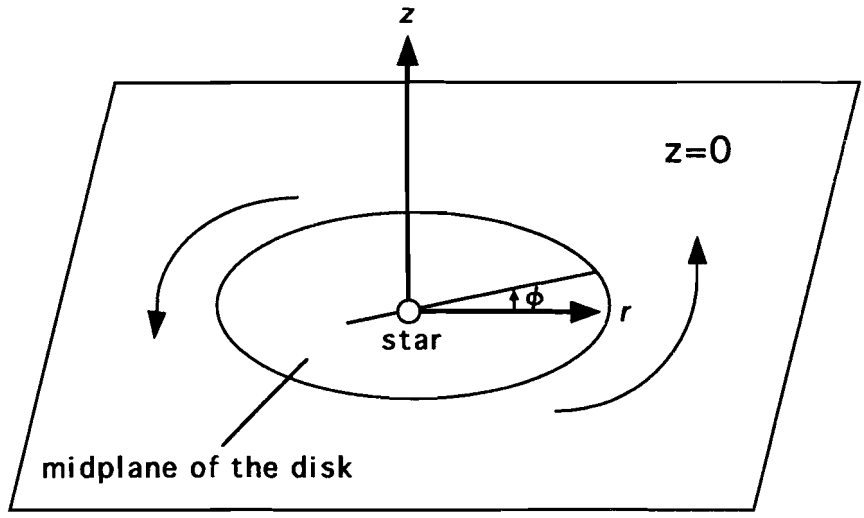

If there is no heat source in a disk, except for surface heating due to stellar light, the disk will become locally isothermal in the vertical direction. With a sufficiently thin disk, heat is more easily transported vertically than radially. The structure of such a disk can be solved analytically by balancing the vertical pressure gradient with the vertical component of central star's gravity. This equalization leads to the density

profile at the distance r from the central star in cylindrical coordinates (r, ϕ, z):

$$\rho(r,z) = \frac{\Sigma(r)}{\sqrt{\pi}H} e^{-(z/H)^2}, \tag{2}$$

where $\Sigma(r)$ is the surface density of the disk and H is the gas scale height. The height represents the level where the gas density is reduced to e^{-1} of the maximum value (the density of the disk's midplane) and this value can be regarded as the half thickness of the disk. The height H can be written with isothermal sound speed $c_s = [kT(r)/\mu m_H]^{1/2}$ and Kepler rotation rate $\Omega_K = (GM_*/r^3)^{1/2}$ as

$$H = \sqrt{2}c_s/\Omega_K. \tag{3}$$

Here k, μ, and m_H are the Boltzmann constant, the mean molecular weight (= 2.34 for the present solar chemical composition), and the mass of hydrogen atom, respectively.

Next the radial structure of the disk is considered. The radial density distribution depends on the radial surface density distribution $\Sigma(r)$, which will be achieved by disk evolution before the disk becomes passive and disk accretion ceases. In this paper, we will adopt as the nominal surface density the surface density distribution of so-called minimum-mass solar nebula,

$$\Sigma(r) \equiv \int_{-\infty}^{\infty} \rho(r,z)dz = 1.7 \times 10^3 \left(\frac{r}{1\mathrm{AU}}\right)^{-3/2} \mathrm{gcm}^{-2}, \tag{4}$$

which is derived from the present solar system by adding H_2 and He gases (Hayashi 1981 [8]). The mass of the disk with this nominal surface density, which extends from stellar surface ($\sim$ 0.01 AU) to 100 AU is estimated to be about 0.02 $M_\odot$. This is consistent with the order of the typical mass of the disks around T Tauri stars derived from observations at optically thin millimeter wavelength (Beckwith et al. 1990 [23]).

However, the surface density $\Sigma(r)$ is a quantity which is difficult to constrain by the present observations because of the lack of spatial resolution. So the general form $\Sigma(r) = \Sigma_1(r/1\mathrm{AU})^{-p}$ for wide ranges of the constants Σ_1 and p should be also considered. Fortunately, however, as was shown in the previous paper of Miyake & Nakagawa (1995) [10], the choice of parameters for the surface density, p and Σ_1 does not affect temperature distributions. Therefore, as long as disks are optically thick for the stellar light, SEDs obtained in this paper do not change with different choices of p.

Next, we consider the radial temperature distribution $T(r)$, which will be determined by the photon flux from the central star absorbed by the disk surface. Here the word *surface* is used to mean the level at which stellar light is absorbed. Previous studies have assumed that the central star's radiation comes from above the disk and is absorbed around the scale height of the disk H (Kusaka, Nakano, & Hayashi 1970 [11]; Ruden & Pollack 1991 [12]) or at $z = 0$ (Friedjung 1985 [13]; Adams & Shu 1986 [14]). In any case, the temperature is determined by the balance of heating by the central star's radiation and cooling by thermal emission. Ruden & Pollack (1991) [12] gave a general formula which determines the temperature distribution of the flaring absorbing surface disks, assuming that the absorbing surface height is equal to the gas scale height H. Using a similar formula to theirs, Miyake & Nakagawa noted that the heating rate depends on the disk geometry. In this paper, we will adopt the formula (Miyake & Nakagawa 1995 [10]) for the radial temperature distribution $T(r)$:

$$\sigma T(r)^4 = \frac{L_*}{8\pi r^2}\left[\frac{4}{3\pi}\left(\frac{R_*}{r}\right) + \left(\frac{H}{r}\right)\left(\frac{d\ln H}{d\ln r} - 1\right) f\right] + \frac{3GM_*\dot{M}}{8\pi r^3}\left(1 - \sqrt{\frac{R_*}{r}}\right), \quad (5)$$

where L_* and R_* are the same notation previously used, M_* is the central stellar mass, and σ and G are the Stefan-Boltzmann and gravitational constants, respectively. The first term of the right-hand side represents the heating due to disk flaring. The factor f represents a correction factor for the difference between the height H and that of the absorbing surface. So, if stellar light is absorbed at the gas scale height then $f = 1$. As will be shown later, $f = 1$ is a rather good approximation of a condition where dust particles are well mixed with gas. As the dust particles sink towards the equatorical plane of the disk, the height of the absorbing surface becomes lower and hence, the value of f-factor decreases to zero. $f = 0$ represents a condition where dust particles have completely settled. The last term of the right-hand side of equation (5) denotes the viscous heating on steady accretion (Lynden-Bell & Pringle, 1974 [15], Shakura & Sunyaev, 1973 [16]). This term will have to be added to examine the effects on the temperature distribution of an intrinsic heat source by mass accretion. But with the passive disks considered in this paper, this term is negligible. According to Kusaka et al. (1970) [11], the temperature distribution of about $T \propto r^{-3/7}$ is achieved if we

neglect the last term of the right-hand side and if we adopt $f = 1$. The possibility of a change in parameter f will be discussed later. Provided $f = 0$, then equation (5) is the same as that derived by Friedjung (1985) [13] and Adams & Shu (1986) [14], except for the last term of the right-hand side. If the last term of the right-hand side is negligible, equation (5) with $f = 0$ will apparently lead to the temperature distribution $T \propto r^{-3/4}$, as was discussed in Adams & Shu (1986) [14]. On the other hand, if only the last term in the right-hand side remains, then the resulting temperature distribution will be the same as the one for the purely reprocessing disk with $f = 0$, $T \propto r^{-3/4}$, which has been discussed by Lynden-Bell & Pringle (1974) [15]. Detailed consideration of temperature distribution of disks is given in also recent studies (Chiang & Goldreich, 1997 [17]).

2.3 Height of the absorbing surface

As we have mentioned in the previous section, previous studies have assumed that stellar light is absorbed at the gas scale height $z = H$, but this assumption is not so obvious. Miyake & Nakagawa (1995) [10] have examined where stellar light is absorbed, and we will introduce their results in this section.

It is quite simple to calculate the height of the absorbing surface for the vertical incidence of light. If the effect of scattering is negligible, stellar light will be absorbed at the optical depth $\tau \sim 1$. We can obtain the optical depth for the vertical incidence by integrating $\rho(z)$ of equation (2) from $z = \infty$:

$$\tau(z) = \int_z^\infty \kappa_{1\mu\mathrm{m}} \rho(z) dz = \frac{\kappa_{1\mu\mathrm{m}} \Sigma}{\sqrt{\pi}} \int_{z/H}^\infty e^{-\zeta^2} d\zeta, \tag{6}$$

where $\kappa_{1\mu\mathrm{m}}$ is the absorption opacity for stellar light, which has the typical wavelength $\lambda \sim 1\mu$m. It should be noted that the absorbing surface is determined by the absorption opacity only at $\lambda \sim 1\mu$m, the value of which is $\kappa_{1\mu\mathrm{m}} \sim 10$ cm^2 g^{-1} for the interstellar dust particles with submicrometer radii. While Draine & Lee (1984) listed the values of extinction opacity, which can be as large as $\kappa_{1\mu\mathrm{m}} = 100$ cm^{2}g^{-1}, but we are interested in absorption opacity here. It is true that the value of the opacity depends on the dust species and its size distribution (Miyake & Nakagawa 1993 [19]). However, even if dust particles grow in turbulent disks through mutual coagulation and have plausible size

distributions, such as power-law ones with the exponents $s \sim 3.5$ and maximum cutoffs $a_{max} \sim 1$ cm in radii (Miyake & Nakagawa 1993 [19]), it is fortunate that $\kappa_{1\mu m}$ is kept almost the same as for interstellar dust particles. Now the height of absorbing surface can be given by solving $\tau(z) = 1$ to be $z \simeq 3H$ (for $\Sigma = 3$ gcm^{-2}) or $z \simeq 2H$ (for $\Sigma = 10$ gcm^{-2}) in the case $\kappa_{1\mu m} = 10$ cm^{2}g^{-1}; then the height of the absorbing surface changes, weakly depending on Σ, but is larger than the gas scale height H by a factor of 2 or 3.

However, in reality, stellar light does not come from above the disks, but rather the disks are illuminated almost at shadow angles. Therefore, not only vertical but also radial structures of the disks should be taken into account in considering the height and shape of the absorbing surface. We numerically calculated the optical depth contour measured from the central stars through the given two-dimensional density distributions of the disks with parameters which are typical ones for passive reprocessing disks around T Tauri stars.

The two-dimensional structure of the vertically isothermal disk $\rho(r, z)$ is determiend only by the surface density distribution $\Sigma(r)$ and the temperature distribution $T(r)$, as in equation (2). Now we assume $\Sigma(r)$ to be the nominal one and the temperature distribution to be $T(r) = 100$ K$(r/1\mathrm{AU})^{-1/2}$ or $T(r) = 100$ K$(r/1\mathrm{AU})^{-3/4}$, which are almost the same as ones achieved for flaring or flat thin passive disks, respectively, as will be shown later. Disks are assumed to extend from the stellar surface R_* to 100 AU, and the mass absorption opacity for stellar light is taken to be $\kappa_{1\mu m} = 10$ cm^{2}g^{-1}. Here R_* denotes the radius of the central star and ~ 0.00994 AU, which is obtained from the assumptions $T_* = 4000$ K and $L_* = 1L_\odot$, the typical values for the Taurus-Auriga cloud complex. Figures 2a and 2b of the paper of Miyake & Nakagawa (1995) [10] show the loci for $\tau_{1\mu m} = 0.1$, 1, 10, 100, and 1000 for the nominal surface density and the temperature distribution $T(r) = 100$ K $(r/1\mathrm{AU})^{-1/2}$. The loci for $\tau_{1\mu m} = 0.1 - 10$ locate above the gas scale height H by factors and have almost the same flaring exponents, $(d \ln z/d \ln r) - 1$, as for H or have slightly lower ones for larger $\tau_{1\mu m}$ and r. It is shown in Figure 2b that the height of the absorbing surface at the innermost part ($r < 10R_* \simeq 0.1$ AU) is very low as compared with R_*.

Figure 3 of their paper also shows the loci of $\tau_{1\mu m} = 1$, or the absorbing surface, for the nominal surface density and two different temperature distributions — $T(r) = T_1(r/1\mathrm{AU})^{-q}$, where $T_1 = 100$ K and $q = 0.5$ and 0.75. They made the power-law fitting of the height of the absorbing surface Z as $Z \propto r^{\gamma}$, for each region 0.01 AU $< r <$ 0.1 AU, 0.1 AU$< r <$ 1 AU, 1 AU $< r <$ 10 AU, 10 AU $< r <$ 100 AU, and show the results also in their Fig. 3.

Now in equation (5) the gas scale height H should originally mean the height of the absorbing surface Z, and equation (5) tells us that the product of Z/r and the flaring exponent $d\ln Z/d\ln r - 1$ ($\equiv \gamma - 1$) determines the efficiency of the disk heating. From Fig. 3 in the case of $q = 0.5$, the height of the absorbing surface is larger than the gas scale height by a factor of 2 or more at the outer part of the disk (say $r > 1$ AU), while the flaring exponent $\gamma - 1$ of the absorbing surface is smaller than that of the gas scale height H in equation (5) as it is; in that case the efficiency is slightly higher in the case of $q = 0.5$ and slightly lower in the case of $q = 0.75$. They have therefore concluded that it is a rather good approximation to take the gas scale height to be the height of the absorbing surface of stellar light. We will also adopt this approximation hereafter. However, it should be kept in mind that $q < 0.5$ is achieved in the cases of flaring passive reprocessing disks, as will be seen later, and hence, adopting the gas scale height as the height of the absorbing surface is somewhat of an underestimation, while the difference in the heating efficiency in equation (5) will be less than a factor of 2.

2.4 Dust particle settling

The most important process that changes the height of the absorbing surface of a disk is dust particle settling. Gas molecules can absorb stellar light only by line absorption, while dust particles can do so by continuum absorption. Thus, stellar light will first heat almost only the dust particles, and then the gas molecules will be heated through collisions with dust particles or through absorption and desorption. Once gas molecules are heated, their cooling time is very long because they can only be cooled by line emission. Hence gas molecules play a very minor role both in heating and cooling

of the disks. Therefore, if the scale height of the dust particles becomes different from that of the gas, the absorbing surface will be determined not by the gas but by the dust particles.

Indeed, if the turbulent gas motion is sufficiently weak, dust particles are supposed to settle towards the midplane by action of the vertical component of the gravity of the central star, but gas molecules will not settle because they are supported by the pressure gradient. Dust particle settling will lead to a lower height of the absorbing surface and will decrease the efficiency of the surface heating by the central star. However, unfortunately, estimating the temporal variation of the height of the absorbing surface is difficult because of our scanty knowlege of the size distribution of the dust particles or the strength of turbulence in the disk.

Here we will discuss the cases of quiescent disks with no turbulence. According to Weidenschilling (1980) [20] and Nakagawa, Nakazawa & Hayashi (1981) [21], particle coagulation and sweep-up of smaller particles by larger ones due to size-dependent settling velocities may accelerate the settling of dust particles. Their numerical calculations show that the settling time is of the order of 10^3 yr and that the final size of typical dust particles is $\sim 1 - 10$ cm at $r = 1$ AU. Nakagawa, Sekiya, & Hayashi (1986) [22] have obtained an analytical expression for the settling time t_s of the typical dust particles in quiescent disks: $t_s \sim 10^3 t_K \propto r^{3/2}$, where t_K is the Keplerian time; it should be noted that this settling time is insensitive to the assumed disk model but is only determined by the dust-to-gas ratio and the Keplerian time. That is, dust particle settling is hightly nonhomologous with respect to r. The transient radial distribution of dust scale height or of absorbing surface height will therefore be quite different from that of gas scale height, but such a transition feature is not so significant because the transition time ($10^3 t_K \sim 10^3 - 10^6$ yr) is rather short as compared with the age of T Tauri stars (10^7 yr). That is, dust particles settle to the midplane promptly after the cessation of turbulence in the disk, and the height of the absorbing surface becomes sufficiently small.

However, if the sweep-up of small particles by larger ones is imcomplete and there remain enough unswept small particles to absorb the central star light, then the de-

crease of the absorbing surface height is controlled by the settling of those small dust particles left above the typical grown ones; this situation seems to hold, judging from the numerical simulations of dust particle settling, taking the size distribution into account, by Weidenschlling (1980) [20] Nakagawa et al. (1981) [21]. For example, Nakagawa et al. (1981) [21] showed by local numerical simulation at $r = 1$ AU that an appreciable amount of dust particles, 1/100 of the total, are left above the midplane ($\geq H/20$) after most dust particles have settled close to the midplane ($t = 10^4$ yr). We should note that small dust particles left above the midplane with mass fraction of only $\sim 10^{-4}$ of the total are necessary to keep the disk absorbing surface flaring, if we adopt the nominal surface density at $r = 1$ AU. We also note that all the processes neglected in the simulation by Nakagawa et al. (1981) [21], such as sticking probability less than unity, fragmentation of dust particles due to mutual collisions, or presence of weak turbulence, will provide smaller dust particles as well as a longer settling time.

Therefore, the settling of these small dust particles may affect the reduction of the absorbing surface height. Miyake & Nakagawa (1995) [10] can obtain the general formulae of the settling time of small dust particles according to Nakagawa et al. (1981 [21], 1986 [22]). For sufficiently small dust particles (where the Knudsen number is larger than unity), Epstein's law of drag force is to be applied to derive the terminal settling velocity as

$$v_z = -(\Omega_K^2/D_r)z, \tag{7}$$

where Ω_K is the Keplerian angular frequency and $1/D_r$ is the characteristic time of drag force: $D_r = \rho c_t/\rho_s a$, where ρ is the gas density, $c_t = (8kT/\pi\mu m_H)^{1/2}$ is the mean thermal velocity of the molecular gas, and ρ_s and a are the material density and the radius of the dust particle, respectively. It should be noted that the molecular mean free path is typically a few centimeters (at $r \sim 1$ AU) and tens of micrometers even at the inner edge of the disk (at $r \sim 0.01$ AU) if the nominal disk parameters are adopted; hence, Epstein's law is appropriate in every part of the disk for dust particles with radii $a \leq 10\mu$m. The timescale for a dust particle to settle from $z = z$ to $z = z_0$ is given by

$$t_s = \int_z^{z_0} \frac{dz}{v_z} = -\frac{\rho c_t}{\rho_s a}\frac{1}{\Omega_K}\int_z^{z_0}\frac{dz}{z} = \frac{\pi}{2}\frac{\Sigma(r)}{\rho_s a}\frac{1}{\Omega_K}\ln\frac{z}{z_0}, \tag{8}$$

where we have replaced the gas density by the midplane gas density $\rho_0 = \Sigma/\pi^{1/2}H = 2\Sigma\Omega_K/\pi c_t$. Now if we adopt the nominal surface density with the exponent for the radial distribution $p = 1.5$, the dependence of t_s on r cancels out between Σ and Ω_K, and we get $t_s \sim 10^7$ yr. This timescale is comparable to the lifetime of T Tauri stars; hence, it is quite probable that we observe the transient stage of dust particle settling. The settling of small dust particles will be rather homologous with respect to the radial distance r; hence, the reduction of the absorbing surface height due to the small-particle settling can be characterized only by one parameter, f, the ratio of the absorbing surface height to the gas scale height. We consider that f is constant with respect to r in deriving the temperature distribution by equation (5).

3 Protoplanetary disks around single young stars

3.1 Model calculations

Figure 6: Radial Temperature Distribution

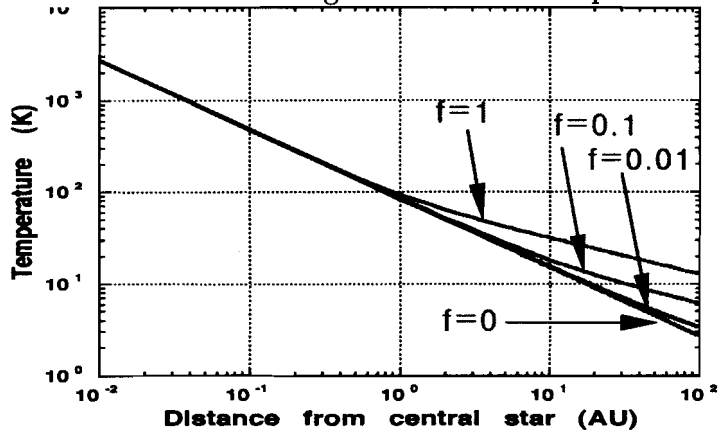

In this section we at first present the results of the numerical evaluation of equation (5). To calculate $T(r)$ with equation (5), we need to know not only H but also $d\ln H/d\ln r$, but they, in turn, depend on $T(r)$. So we performed an iterative procedure to get $T(r)$ for $f \neq 0$. As for the parameters of the central star, we adopt the typical values for T Tauri stars in the Taurus-Auriga cloud complex (Beckwith et al. 1990 [23]): $T_* = 4000$ K, $L_* = 1\ L_\odot$, and $M_* = 1\ M_\odot$. With these parameters, we obtain $R_* = (L_*/L_\odot)^{1/2}(T_*/T_\odot)^{-2}\ R_\odot = 2.08\ R_\odot \simeq 0.01$ AU. Disks are assumed to extend from the surface of the central star to $r = 100$ AU. First, we examine the effects of the parameter f on the temperature distribution, so we fix $\dot{M}$ to be zero (purely passive disk with no mass accretion). In Fig. 6 we show the temperature distributions of passive reprocessing disks ($\dot{M} = 0$) for various f- factors. From Fig. 6 it is understood that the power-law exponent of temperarture distribution with respect to r ($T \propto r^{-q}$) is almost $q = 0.75$ for $r < 1$ AU even for $f = 1$ and decreases toward $q = 0.5$

for larger r. The exponent $q = 0.75$ for small r is expected for flat thin disks heated by the central star with finite dimension (Adams & Shu 1986 [14]). The turnover distance increases with decreasing f. For sufficiently small $f < 0.01$, the exponent q is about 0.75 almost all over the disk, and disk flaring is no longer important for determining the temperature distribution of the disk.

It should be noted that the temperature at $r = 1$ AU, T_1, reaches ~ 100 K only by the surface heating from the central star with typical parameters; T_1 for many T Tauri stars observed in the Taurus-Auriga cloud complex are known to range from 100 K to 150 K, from SEDs (Beckwith et al. 1990 [23]).

To compare our models with observations, we have also calculated the SEDs of our theoretical passive disk models. If we assume that the disk is vertically isothermal, then the luminosity density L_ν ($= 4\pi D^2 \nu F_\nu$, where D is the distance from the source and F_ν is the flux density to be observed for the star-disk system viewed at the angle θ [$\theta = 0$ is face-on]) can be expressed as follows (Beckwith et al. 1990 [23]):

$$L_\nu = 4\pi \cos\theta \int_{R_0}^{R_d} \nu B_\nu(T)(1 - e^{-\tau_\nu}) 2\pi r dr + L_{\nu *}, \tag{9}$$

where B_ν is the Planck function, the slant optical depth τ_ν is given by

$$\tau_\nu(r) = \kappa_\nu \Sigma(r) / \cos\theta, \tag{10}$$

$L_{\nu *}$ is the stellar component of L_ν and R_0 and R_d are the inner and outer radii, respectively. Note that L_ν does not depend on the choice of the opacity κ_ν as long as $\tau_\nu \gg 1$. In the following calculations, we use the absorption opacity for dust particles of radius $a = 1$ μm of Miyake & Nakagawa (1993) [19], where the assumed dust species is only silicate for the regions where $T > 160$ K and silicate plus H_2O ice for the regions where $T \leq 160$ K. That opacity curve is almost identical with the standard interstellar extinction curve by Draine & Lee (1984) [18], except for the contribution of H_2O ice, and hence, it will be convenient to compare our results with the results of other researchers. If dust particles have grown to have some size distributions [e.g., $n(a) \propto a^{-s}$ with $s \sim 3.5$ and $a_{max} \sim 1$ cm], the luminosity density L_ν for submillimeter and millimeter wavelengths will change. However, we are mostly concerned with SEDs

at infrared wavelengths ($\lambda \leq 100$ μm), where $\tau_\nu \gg 1$; then, a detailed feature of the adopted opacities does not affect the following results.

Figure 7: Luminosity Density

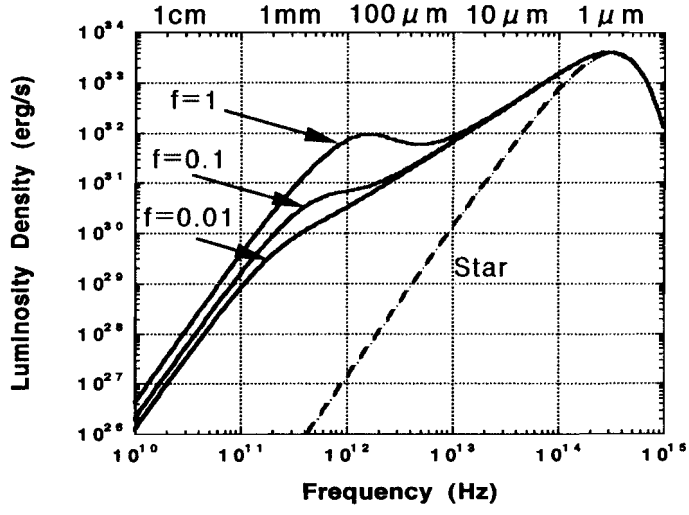

Figure 7 shows the results of our calculation with equation (9). That is, we show the SEDs of passive reprocessing disks ($\dot{M} = 0$) for various f-factors. Now we define the spectral index $n = d\ln L_\nu / d\ln \nu$ at infrared wavelengths, which is 3 for the stellar blackbody radiation and is known to range widely from slightly greater than unity to zero for T Tauri stars (Rucinski 1985 [24]). In the case of optically thick thermal emission from the disk, the spectral index n can be expressed with the exponent of the temperature distribution q as $n = 4 - 2/q$ (Beckwith et al. 1990 [23]). According to Fig. 7, the spectral index n for sufficiently small $f < 0.01$ is $\sim 4/3$ for wide range

of frequency $10^{12.5} - 10^{14}$ Hz, which is the natural consequence of the temperature distribution for $q = 0.75$. For $f = 1$, however, we see considerable enhancement in the SED, by almost an order of magnitude, and a null or negative index $n(\leq 0)$ around $\nu \sim 10^{12.5}$ Hz (i.e., $\lambda \sim 100$ μm), although at $\nu > 10^{13}$ Hz (i.e., $\lambda < 30$ μm) there is no difference in the spectral indices when f changes from 0.01 to 1.

Now it should be noted that there are uncertainties in the observed apparent disk luminosity due to the unknown viewing angle θ and that available data are almost restricted to $\lambda < 100$ μm, except for a few well-studied stars. Thus, we may not distinguish f-factors definitely from the observations. Anyway, we can compare the calculated SEDs for $f = 1$ and $f = 0$ directly with observations.

3.2 Sample single stars

In this section we list the main properties of sample young stars used in our calculation. Many new stars, which are interpreted assuming that the emission is thermal radiation from small particles entrained in circumstellar disks, have been discovered by recent observation. A significant number of stars which were treated as isolated single ones are now known to be binary or multiple. All sample stars dealt with in this section, however, are limited to isolated single stars. The only exception V826 Tau is a spectroscopic binary ($P = 3.9$ d), but it is formally considered as unresolved system (Mundt et al. 1983 [25]; Reipurth et al. 1990 [26]). We will comment on sample stars in binary or multiple systems in section 4.2.

The sampling is based on the Herbig-Bell catalogue (Herbig-Bell, 1988, hereafter HBC [27]). We also checked new candidates discovered in the surveys of Gomez et al. (1992) [28] and Hartmann et al. (1991) [29] or selected by these authors from the list of Jones & Herbig (1979) [30]. All of the unmeasured sources compiled in Leinert et al. (1993) [31] survey for multiple stars were included, as well as the "naked" T Tauri stars of Walter et al. (1988) [32]. Naked T Tauri stars are presumed to have little or no disk material and hereafter collectively referred to as WTTSs. In addition to these data, Osterloh & Beckwith (1995) [7] included several YSO classified as Herbig AeBe stars (Herbig 1960 [33]), FU Orionis stars (Herbig 1977 [34]), SU Aur stars — high

luminosity, weak Hα and Ca II emission, very broad absorption lines (HBC) and IRAS sources, as well as objects from different regions of the sky. In this paper, we combined data of IRAM observation which were compiled in the paper of Osterloh and Beckwith (1995) [7] with the previous data of IRAS (IPAC 1986; Strom et al. 1989 [41]).

Now we briefly comment on the observational data which are referred to in this paper. InfraRed Astronomical Satellite (IRAS) was a joint US (NASA), the Netherlands (NIVR), and the United Kingdom (SERC) project. IRAS conducted an all-sky survey at wavelengths ranging from 8 to 120 microns in four broadband photometric channels centered on 12, 25, 60 and 100 microns. Following a 10 months long mission, IRAS exhausted its cryogen and ceased operations on November 21, 1983. Some 250,000 well-confirmed infrared point sources were detected and presented in IRAS catalogue of Point Sources, Version 2.0 (IPAC 1986). Raw data of positions, flux densities, uncertainties, associations with known astronomical objects and various cautionary flags are given for each object in this catalogue. Where two stars fall within the IRAS beam Strom et al. (1989) [41] have divided the observed 12 and 25 μm IRAS fluxes in propotion (respectively) to the 10 and 20 μm fluxes measured from the ground (if both are available), and in proportion to the 10 μm measurements if 20 μm measurements are unavailable; the 60 and 100 μm fluxes have been divided between the two stars in proportion to the longest-wavelength ground-based IR measurements available. Weaver & Jones (1992) [35] also provide us some upper limits of IRAS fluxes. As for the sources which lack adequate optical or near-IR photometry, we adopt raw IRAS fluxes with no color corrections. The IRAM (Insitut de RadioAstronomie Millimetrique) observations were performed during the nights December 2-6 1993 with the 30 m IRAM telescope at Pico Veleta. The detector was the IRAM single-channel bolometer operating at 1.3 mm as described by Thum et al. (1992) [36]. When combined with the earlier work of Beckwith et al. (1990) [23], the data of millimeter-wave observations are extended to 121 objects (Beckwith et al 1995 [7]). There are now millimeter wave observations of almost all known T Tauri stars in Taurus-Aurigae dark clouds and new observations of several other young stellar objects of various masses and subclasses. Especially significant is the inclusion of many binary and multiple systems and weak-line T Tauri stars.

Spatial resolution of IRAS data is poor in comparison with that of recent observations, such as IRAM. Our sample stars comprise some sources which were not resolved by IRAS observation (for example, XZ Tau & HL Tau, V807 Tau & GH Tau, $\cdots$).

In Table 1 we present the data of sample single stars used in our calculation. We give each source name in the first column denoting the head number with the corresponding the HBC number. If the stars are located in Taurus-Auriga cloud complex, they are flagged by an asterisk (*) following the source name. One source marked by a dagger (†) is located in L1473 and two sources by (‡) are in L1642. Sources without flags are miscellaneous. Stellar type of each source is assigned according to the HBC. For HBC stars without Hα measurements, spectral types are listed instead of stellar ones. The distance (pc) from the source is listed in the third column. No entrance in the distance column for Taurus-Auriga members means that a distance of 140 pc is assumed (Elias 1978 [37]). In the last three columns we present stellar parameters required in our calculation according to Osterloh & Beckwith (1995) [7]. Stellar luminosities L_* and masses M_* are written in factors unit of solar ones, respectively.

It should be noted that there are potentially large uncertainties in determining L_* from observed fluxes, which are contaminated by the veiling emissions from boundary layers and infrared emissions from circumstellar disks. Indeed, different authors report stellar luminosities different by a factor of 2 or 3 with different manners of reduction. The values of L_* listed by Beckwith et al. (1990) [23] are in good agreement with those obtained through detailed spectroscopic observations by Hartigen et al. (1991) [38], so we adopted the stellar properties listed in Beckwith et al. (1990) [23]. We also adopted the data of their new paper (Beckwith et al. 1995 [7]), which broadens the sample of their previous paper to include WTTSs, multiple systems, and a number of higher mass objects. The stars have been dereddened using a standard reddening law (Cardelli, Clayton, & Mathis 1989 [39]). Effective temperatures, T_*, were assigned to spectral types according to Cohen & Kuhi (1979) [40]. The stellar radius, R_*, were determined by least-squares fitting of the dereddened *absolute* photometric magnitudes. Stellar luminosities were calculated from the effective temperature and radius assuming a Planck distribution: $L_* = 4\pi R_*^2 \sigma T_*^4$.

Table 1: Sample single stars

Source Name	Type	D (pc)	L_*	$\log(T_*)$	M_*
33 DE Tau*	CTT		1.21	3.566	0.5
75 DS Tau*	CTT		1.32	3.679	1.0
381 Haro 6-5B*	CTT		-	3.500	0.1
385 IP Tau*	M0:V		0.48	3.593	0.6
393 L1551 IRS5*	K2 III		27	3.695	1.0
399 V827 Tau*	WTT		1.30	3.602	0.6
400 V826 Tau*	WTT		1.13	3.602	0.6
404 V807 Tau*	CTT		5.25	3.602	0.6
405 V830 Tau*	WTT		0.81	3.602	0.6
411 CK Tau-Aur 3*	WTT		0.09	3.566	0.4
421 CK Tau-Aur 4*	WTT		0.22	3.555	0.4
419 LkCa 15*	WTT		0.87	3.643	1.0
428 V347 Aur*	WTT		4.36	3.544	0.3
429 V836 Tau*	WTT		0.65	3.602	0.7
1 MacC H12	A5, Fe	845	145	3.830	2.5
5 MacC H9	CTT	845	6.20	3.660	1.4
20 LkHa 330	CTT	400	32	3.758	2.5
325 V376 Cas	AeBe	950	-	4.140	>2.5
326 MacC sH15	CTT	845	39	3.710	2.5
328 MC 4	CTT	845	17	3.660	1.4
346 SVS 13	K?	350	2.2	3.719	1.0
363 PP 13s†	M	350	-	3.494	0.15
410 L1642-2‡	CTT	100	-	3.602	0.6
413 L1642-1‡	M	100	-	3.494	0.15
695 RNO 124	?	500	12.30	3.679	1.6
696 PV Cep	AeBe	500	117	3.917	3.3

3.3 Results with sample single stars

We show a detailed comparison between the calculated SEDs based on our passive disk model and the observations of IRAS wavelengths and of millimeter wavelength (λ = 1.3 mm) by Beckwith et al. (1995) [7]. From equation (9) it is understood that $T(r)$, $\Sigma(r)$, θ, R_0, and R_d should be specified for the calculation of SED of each star. We assume that disks have no inclination ($\theta = 0$) and extend from $R_0 = R_*$ to

$R_d = 100$ AU. The radial temperature distribution $T(r)$ is determined from the stellar properties L_*, T_*, and M_* by equation (5) if disk parameters f and $\dot{M}$ are given. Here we consider purely passive disks having no accretion ($\dot{M}$=0).

We show the results of our fitting of observations by passive reprocessing disk model with flaring ($f = 1$) and without ($f = 0$). It is found that a considerable number of our sample T Tauri stars can be well fitted by the passive disk model. There are some uncertainty factors, such as inclination angle of the disk θ or contamination of flux from other sources. The latter is due to poor spatial resolution of IRAS observation as we have mentioned in section 3.2. In spite of these factors, our passive disk model fitting seems to be excellent.

In Figures below we show SEDs of young stars with circumstellar disks well fitted by the passive disk model for $f = 1$ or $f = 0$. The solid triangles represent luminosity densities estimated from observed fluxes by IRAS (IPAC 1986; Strom et al. 1989 [41]) and by IRAM (Beckwith et al. 1990 [23], 1995 [7]). Examples of our spectral fitting are confined to those from single isolated young stars surrounded by circumstellar disks in this section.

Radiation spectra from the single CTTSs are shown from Fig. 8 to Fig. 11 as the representative. Observed data of MacC sH15 and PV Cep are high above the theoretical curve predicted by the flaring disk ($f = 1$) model (Fig. 8, Fig. 9). Disks of these sources are considered to be active ones and have some intrinsic heat source. These two sources correspond to the typical to the typical examples of CTTSs surrounded by active disks. Luminosity densities estimated from observed fluxes of DE Tau are well-fitted by the theoretical curve of $f = 1$ (Fig. 10). This source corresponds to the flaring disk in which dust particle settling has not occurred yet. V807 Tau is unresolved with GH Tau for the IRAS beam. In V807 Tau the observational data exhibit slight deficit from the theoretical curve of $f = 0$. DE Tau and V807 Tau are attributed to the CTTSs surrounded by passive reprocessing disks.

Radiation spectra from WTTSs are given from Fig. 12 to Fig. 15. V347 Aur, the appearance is that of a star-disk system seen edge-on, although our fitting is the case of the pole-on. The only source with detected mm emission classified as a WTTS by

the HBC is LkCa 15; yet it has $ew(\mathrm{H}_\alpha) = 13$ Å (see HBC and references therein), thus not representing a typical WTTS. Luminosity densities estimated from observed fluxes of both V347 Aur and LkCa 15 are plotted above the theoretical curves of $f = 1$. We can consider that the dust particle has not started yet and there is some heat source in the disks of these sources. These sources are considered to WTTSs having active disks. In V836 Tau observed SEDs are well fitted by the theoretical curve of the flat thin disk ($f = 0$) model (fig. 14). V830 Tau exhibits significantly lower fluxes than the $f = 0$ curve. Two plausible interpretations of this are as follows. First, the inner edge of the disk is expected to be larger than the stellar radius (formation of the optically thin inner hole). Second, planetary formation has already started and macroscopic bodies are formed in the inner region.

3.4 Verification of the standard model

According to the results of fitting observed SEDs by our passive disk models, we have found many passive disk candidates can be divided into subclasses of (I) flaring disks, (II) flat thin disks, and (III) disks with inner holes, as summarized in Table 3.

Table 3: T Tauri stars fitted by passive disk models and their properties

Class	Sources	$ew(\mathrm{H}_\alpha)$ (Å)	$\log t$ (yr)
(I)	63 AA Tau	37	6.01
(I)	71 GO Tau	81	6.73
(I)	33 DE Tau	54	5.40
(I)	65 DN Tau	12	5.81
(I)	419 LkCa 15	13	6.30
(II)	28 CY Tau	70	5.87
(II)	65 DF Tau	54	5.00
(II)	75 DS Tau	59	6.78
(II)	46 ZZ Tau	16	6.29
(II)	404 V807 Tau	13	5.84
(II)	429 V836 Tau	9	6.48
(III)	405 V830 Tau	3	6.20
(III)	400 V826 Tau	2	5.90
(III)	399 V827 Tau	2	5.80
(III)	47 V927 Tau	5	5.42

In Table 3 we list the stellar and disk properties of our sample T Tauri stars fitted with passive disk models of each class. The results of Miyake & Nakagawa (1995) [10] are also included in this Table 3. Among the sample stars of Miyake & Nakagawa (1995) [10], we subtract the stars which are indentified as the component of binaries or multiples. Assignment of individual stars to each subclass is, however, somewhat ambiguous because of continuous transition between classes.

From Table 3 we can assess differences in the central star or disk properties among classes. Between class I and II, we cannot find any clear difference (see Table 3). We note that most of members of these classes have $ew(\mathrm{H}_\alpha) > 10$ Å — i.e., they are CTTSs — and that, to the contrary class III includes WTTSs only.

Figure 8: MacC sH15

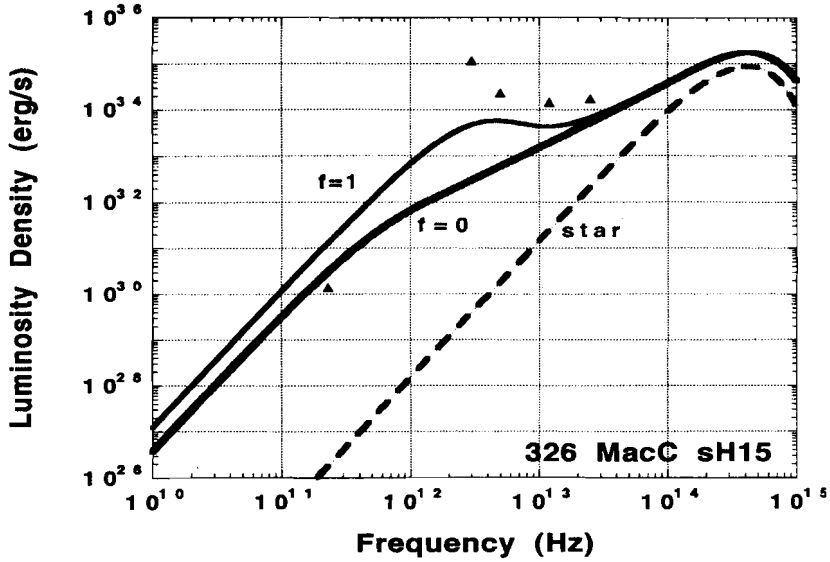

Figure 9: PV Cep

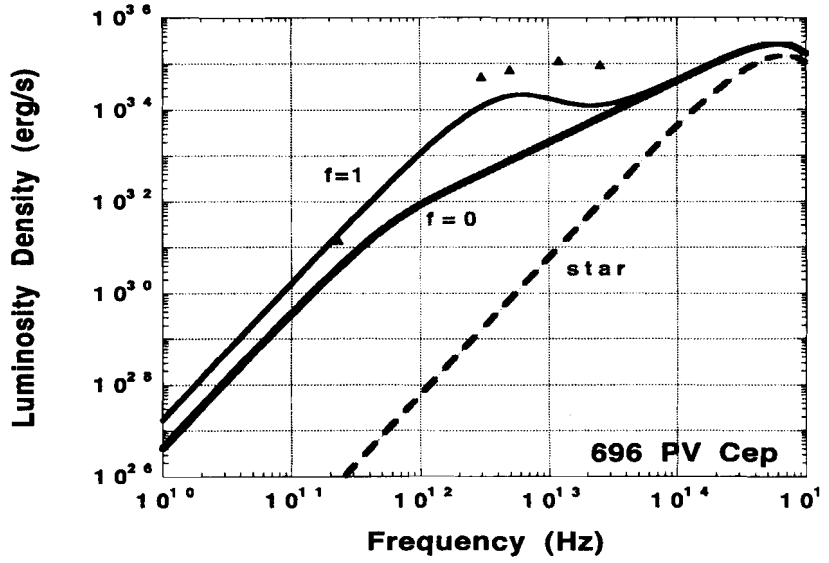

Figure 10: DE Tau

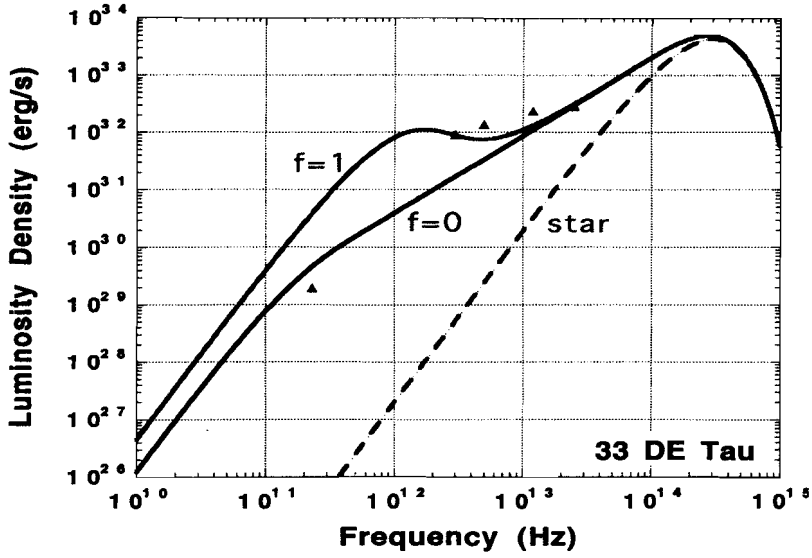

Figure 11: V807 Tau

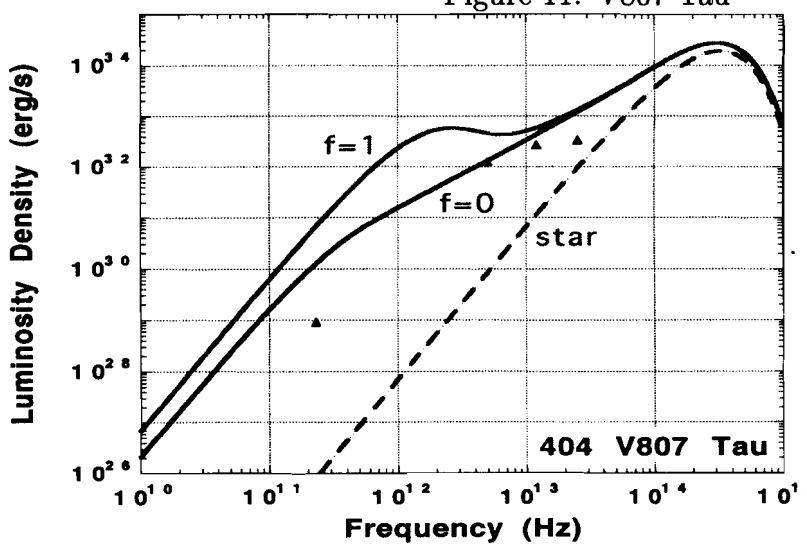

Figure 12: V347 Aur

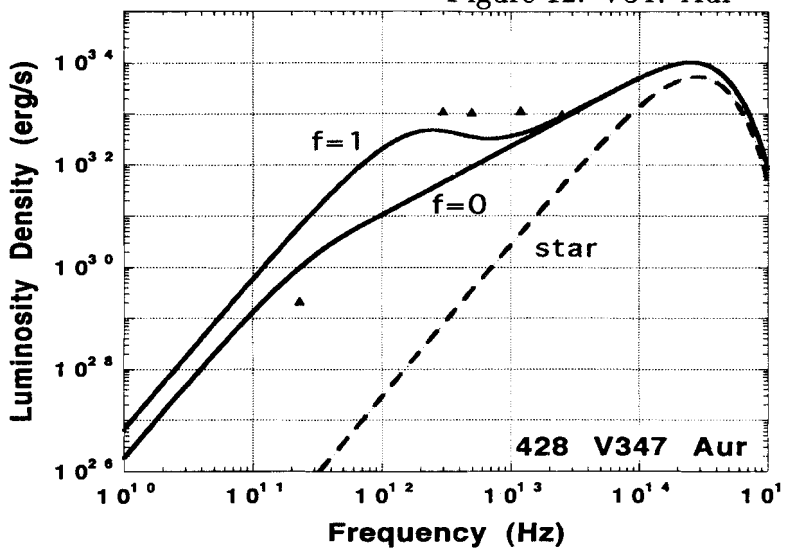

Figure 13: LkCa 15

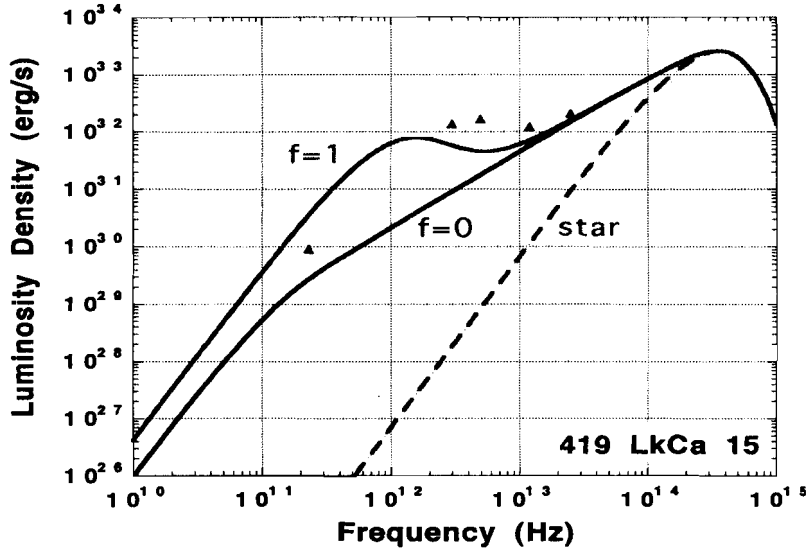

Figure 14: V836 Tau

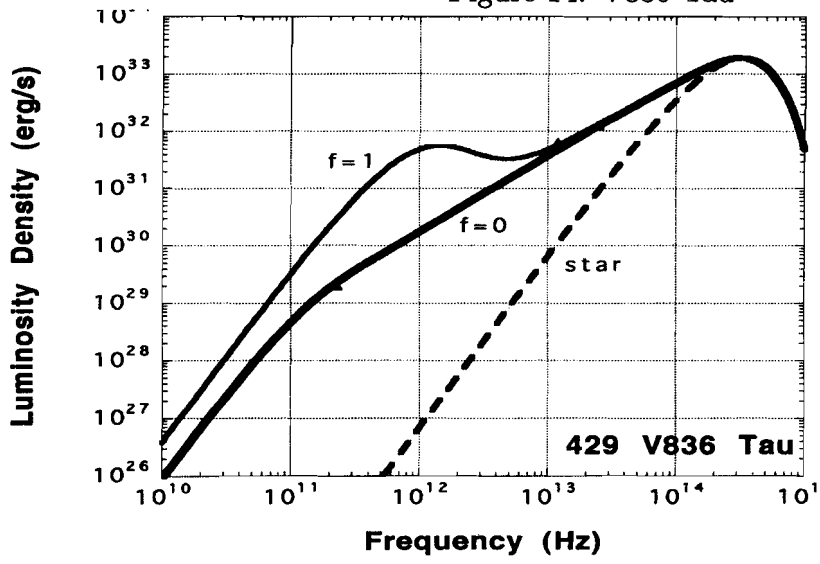

Figure 15: V830 Tau

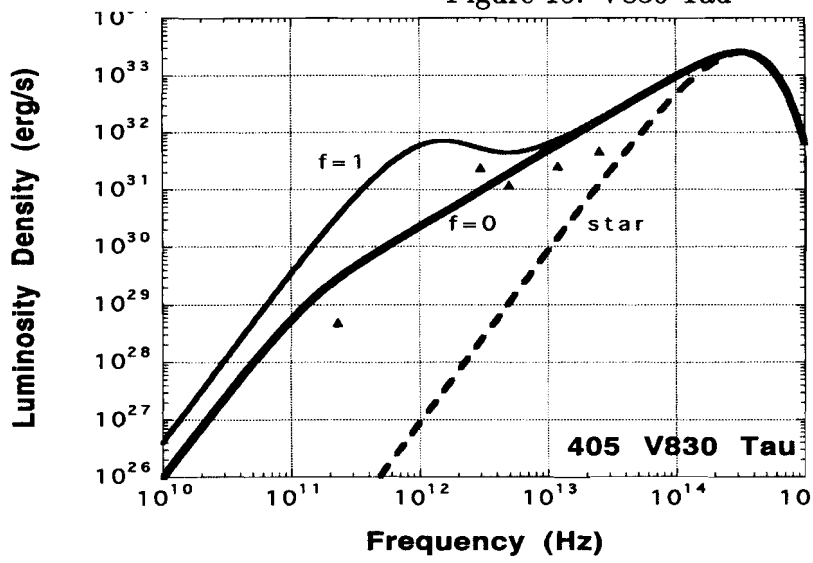

4 Disks around young binaries or multiples

4.1 Basic assumptions

In this section we first mention the difference of disk structure between in close and wide binaries. Figures 16 and 17 present schematic views of a circumstellar disk around a close binary and that of a wide binary, respectively.

Figure 16: Disks in close binaries

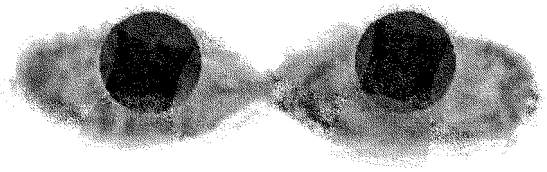

Figure 17: Disks in wide binaries

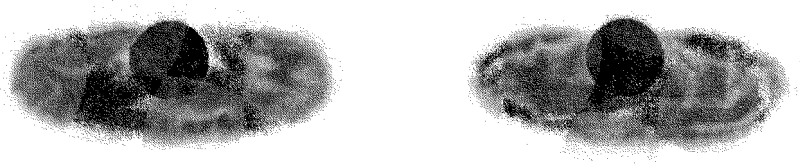

In a close binary the companion star will disrupt stable orbits of all particles on scales from a few tenth of the separation to few times the separation, by the classical *three body* problem. Only disks whose outer radii are much smaller than the separation or whose inner radii are much larger (circumbinary disks) should be stable. Otherwise, disk materials will be filled with Roche lobes around the binary (Fig. 16). An inner gap might be formed around a narrow part of the disk. Gravitational perturbation from the companion prevents dust particles in the disk from settling to the central plane. On the other hand, in a wide binary gravitational effects on the disk from a companion is rather weaker than in the case of a close binary. Disks formed around wide binaries are considered to be relatively similar to ones surrounded by single stars.

It is beyond the scope of this paper to manipulate the temperature distributions taking the disk morphology into consideration. Moreover, stellar properties of the companion are still unknown, as we will mention in section 4.2. We treat both of the component stars in the binary system as the same ones having the same stellar properties in our calculation. We also assume the binary separation is large enough to neglect the heating from the companion.

4.2 Sample stars in binaries or multiples

In this section we list the data of sample binary or multiple young stars in Taurus-Auriga molecular cloud complex according to Leinert et al. (1993) [31]. Ideally we would like to select a complete sample: all young stars in the Taurus-Auriga region whose stellar properties are well known. As we can see from Table 2, stellar types of companions are still unknown in many systems. For practical reasons, and in order to maintain a minimum of homogeneity, we limited ourselves to objects in contained in the HBC of young stars (Herbig & Bell 1988 [27]).

Table 2 lists the data of sample binary stars used in our calculation. Source names and stellar parameters (L_*, T_*, and M_*) are written using the same notation as Table 1 in section 3.2. Projected separations of component stars of each binary are given in AU units. The original values listed in Leinert et al. (1993) [31] were given in seconds. We can easily convert them into the values measured in AU units by multiplying 100 in case of stars in Taurus-Auriga molecular cloud complex. If the star is the component of multiple, we choose the minimum value as the representative separation. We give the stellar type of known component stars of each binary in the third column. Within our sample binary stars, 3 triples (UX Tau, UZ Tau and HV Tau) and 1 quadraples (FV Tau) are included. IS Tau, which was twice unresolved by lunar occultations and resolved by speckle interferometry, is formally considered as unresolved object. There are a few sample stars whose stellar properties are unknown. For example, L_* of FV Tau, M_* of Haro 6-10, and L_* and M_* of HV Tau (see Table 2). We assume that $L_* = 1L_\odot$ and $M_* = 1M_\odot$ in computing SEDs of these sources.

Table 2: Binary and multiple stars in Taurus-Auriga cloud complex

Source Name	Separation	Type	L_*	$\log(T_*)$	M_*
367 V773 Tau	17 ± 1	WTT/?	7.68	3.695	2.0
369 FO Tau	16.5 ± 0.5	CTT/?	1.75	3.544	0.3
30 DD Tau	57 ± 3	CTT/?	1	3.566	0.4
42/43 UX Tau ABC	270 ± 10	WTT×3	2.74	3.695	1.1
44 FX Tau	91 ± 1	CTT/?	0.96	3.566	0.44
50 XZ Tau	30 ± 2	CTT/?	1.55	3.526	0.3
51/395 V710 Tau AB	324 ± 10	WTT/CTT	1.60	3.566	0.4
52/53 UZ Tau ew	34 ± 6	CTT×3	1.60	3.566	0.42
59 IS Tau	21 ± 2	CTT/?	3.1	3.695	1.58
60/406 HN Tau	310 ± 10	CTT/CTT	0.33	3.590	0.7
68 VY Tau	66 ± 2	CTT/?	0.73	3.593	0.6
69 V955 Tau	33 ± 3	CTT/IRS	2	3.602	0.6
73/424 Haro 6-37	270 ± 10	CTT/CTT	2	3.602	0.6
76 UY Aur	89 ± 1	CTT/?	1.88	3.602	0.6
80/81 RW Aur AB	15 ± 1	K3/CTT	7.58	3.708	1.6
378 V819 Tau	1050 ± 300	WTT/?	0.95	3.602	0.72
386/387 FV Tau/c	72 ± 10	CTT×4	-	3.643	1.0
389 Haro 6-10	121 ± 4	K3,5/?	2.2	3.679	-
418 HV Tau	3.5 ± 0.2	WTT/?	-	3.544	-
420 IW Tau	27 ± 2	WTT/?	1.37	3.602	0.6

4.3 Results with sample stars

In this section we show the spectral fitting of young stars with circumstellar disks in binary or multiple systems in the order from more flaring to less.

Luminosity densities estimated from observed fluxes of V955 Tau is well-fitted by our passive flaring disk ($f = 1$) model (Fig. 18). 422 LkHa332/G2 and 423 LkHa332/G1 lie within the IRAS beam for V955 Tau and the total IRAS flux has been assigned to V955 Tau. Although the comment on this source by Osterloh & Beckwith (1995) [7] is that an inner gap has to be assumed ranging out to 4 stellar radii, this gap is not taken into account in our calculation. In UY Tau observational data exhibit much larger luminosities than the theoretical curve predicted by the flar-

ing disk ($f = 1$) (Fig. 19). We should consider some intrinsic heat source such as viscous heating caused by turbulence inside the disk. We can consider that dust particle settling has not started yet in the disks of these systems.

In V773 Tau (Fig. 20) and V710 Tau (Fig. 21) observed data can be well-fitted by the flared disk ($f = 1$) model. IRAS flux measurements of V710 Tau refers to both components A and B of the double. We can consider dust particle settling has not started yet in these sources. There is no difference between the $f = 0$ curve and the curve of the blackbody radiation from the central star in these sources. HN Tau (Fig. 22) and DD Tau (Fig. 23) have significantly larger luminosities than predicted by our passive disk model. While the contribution from nearby object named CZ Tau could be measured separately from DD Tau on the ADDSCAN traces, their intensity position profiles did overlap. Thus, the disks of these sources are considered to be an active disks. In the paper of Miyake & Nakagawa (1995) [10] the spectrum of HN Tau is well-fitted by the case for $f = 1$ and $\dot{M} = 1.7 \times 10^{-7}\ M_{\odot}\ \mathrm{yr}^{-1}$. We ignored the IRAS 100 μm data in SEDs fitting of some sources. There are several plausible explanations for excess emission at 100 μm. Emission from an extended, cold halo (Natta 1993 [42]) or from the molecular cloud might all contribute substantially to the IRAS 100 μm data.

Haro 6-37 (Fig. 24) is well fitted by our model in the case of $f = 0$. According to Osterloh & Beckwith (1995) [7], this source is an example of a consistent picture of a star and a nearby standard reprocessing disk ($q = 0.65$). FO Tau (Fig. 25) also gives a well-fitted example with the $f = 0$ curve.

RW Aur (Fig. 26) and UX Tau (Fig. 27) cannot be fitted by a single parameter of f. This is considered to be due to occurence of mass accretion or contribution of a companion star. The observed IRAS fluxes of UX Tau refers to both components A and B. Since A is much brighter than B in the near-infrared, the total IRAS flux has been assigned to A for the purposes of computing L_{tot}. The near-IR excess of UX Tau can be accounted for through the first IR companion found by Leinert et al. (1993) [31].

4.4 Discussion

In this section we first comment on Fig. 1a of Osterloh and Beckwith (1995) [7] which shows the correlation between the separations of binaries and their flux densities at 1.3 mm (Fig. 28). Projected separations are according to Leinert et al. (1993) [31] of members of multiple systems. Open circles denote binary members and crosses stand for objects in systems consisting more than two components (triples, quadraples, $\cdots$). Systems which are known to have more than two components are treated as a separate sample. Their smallest projected separations are chosen for the abscissa in Fig. 28.

In order to make a comparison, flux densities of the isolated stars of the Leinert et al. (1993) [31] sample arbitrary ordered on x-axis are shown (Fig. 29). From these Figures and some statistical tests performed by Osterloh & Beckwith (1995) [7], we can understand that binary separation has an effect on particle emission from these stars, and that single stars are more likely to have strong emission than binaries. These conclusions also hold, if members of multiple systems with more than two components are included in the samples. It is supposed that the binary and multiple systems will have disk properties differing from those of single stars, since the gravitational field of the companion(s) will perturb the orbits of the disk material.

Now we would like to investigate the correlation between the projected separations of binaries and the settling degree of dust particles in disks. In Fig. 30 we plotted the best-fitted f-factors of sample stars against projected separations. Contrary to our prediction that if the separation is closer, f-factor increases, we cannot find any significant correlation between these two values. A few plausible interpretations are possible as we discuss in the chapter 5.

Figure 18: V955 Tau

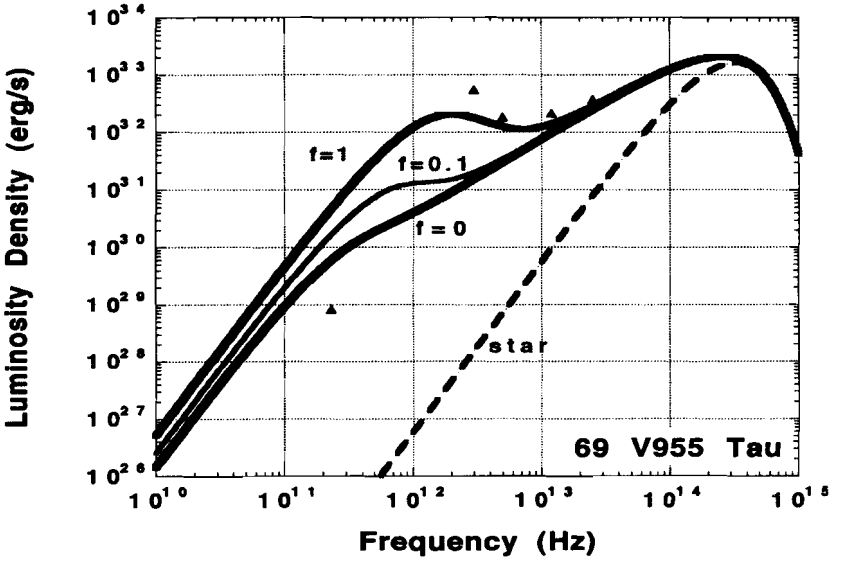

Figure 19: UY Tau

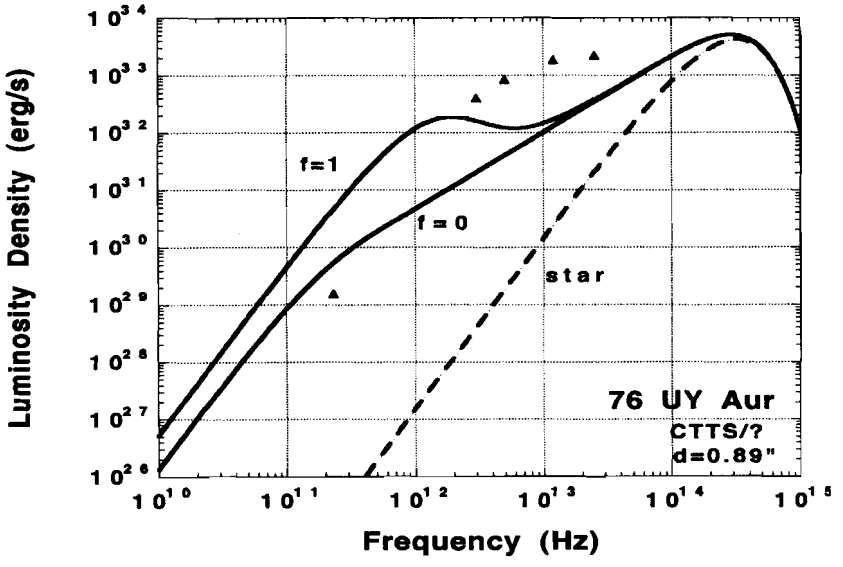

Figure 20: V773 Tau

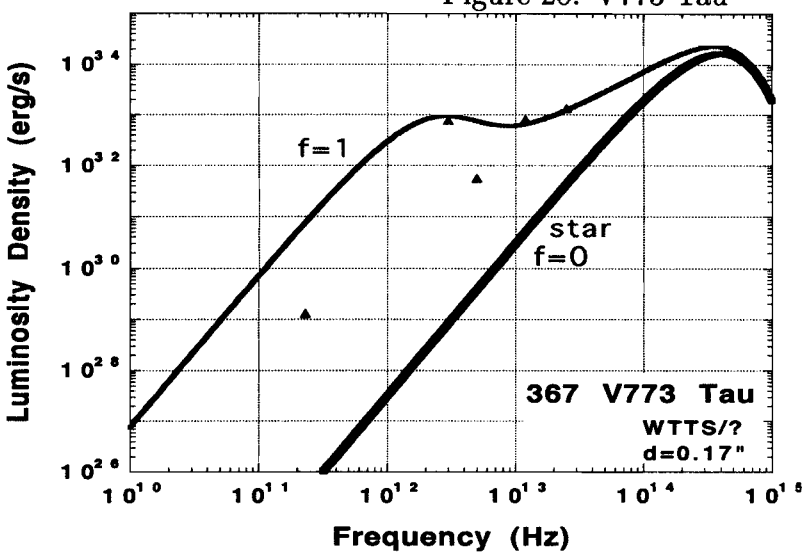

Figure 21: V710 Tau

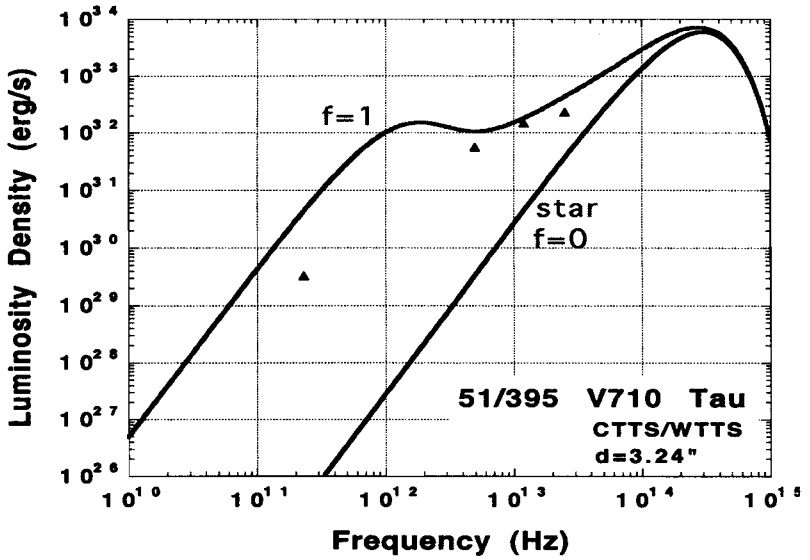

Figure 22: HN Tau

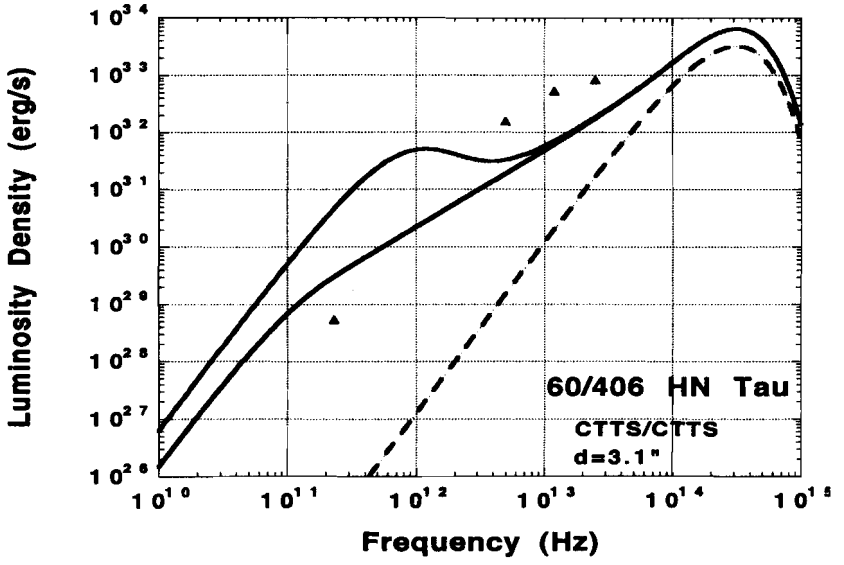

Figure 23: DD Tau

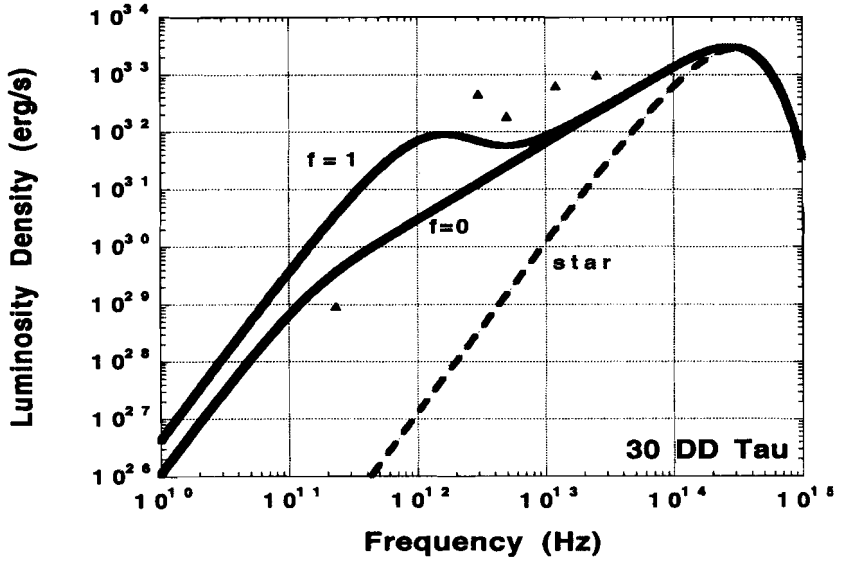

Figure 24: Haro 6-37

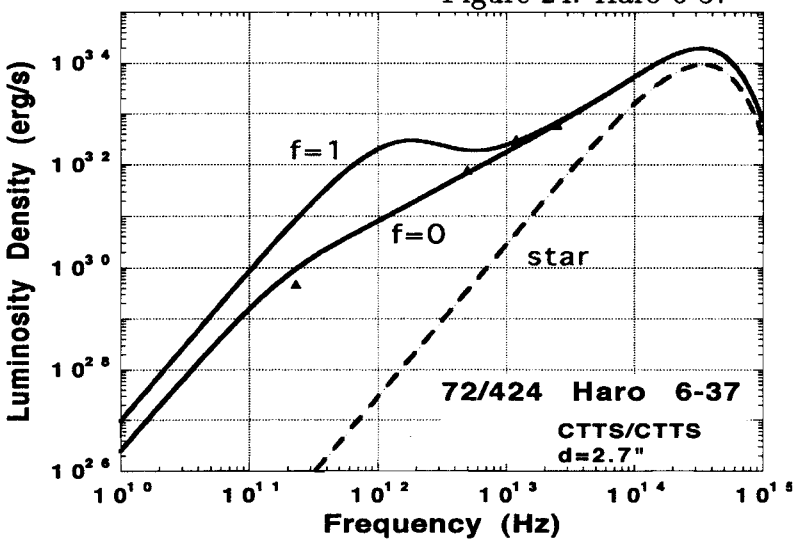

Figure 25: FO Tau

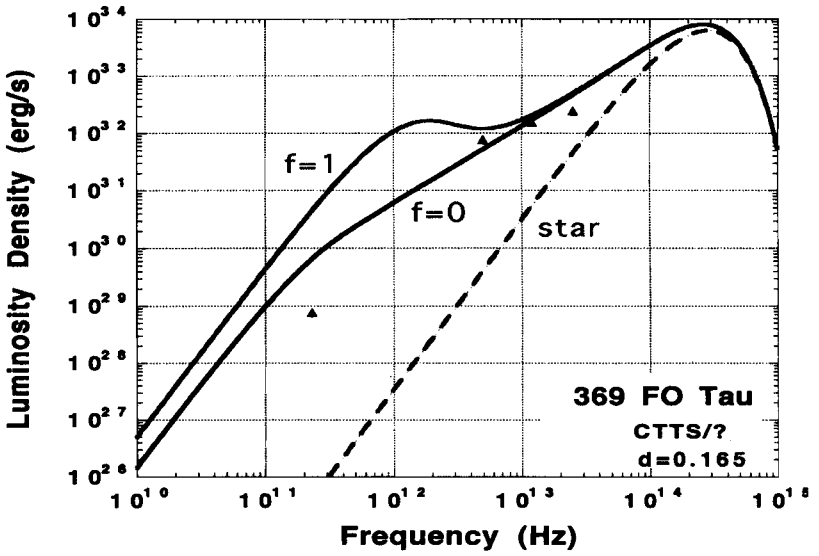

Figure 26: RW Aur

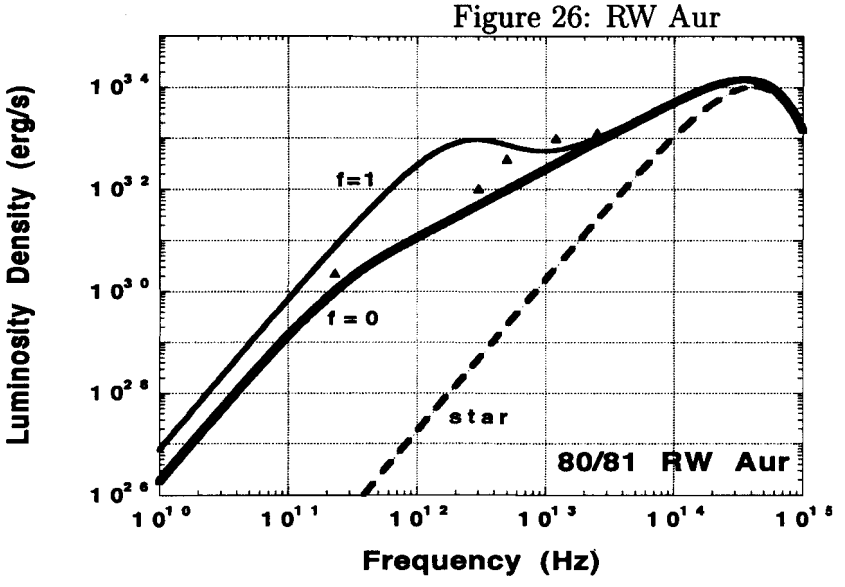

Figure 27: UX Tau

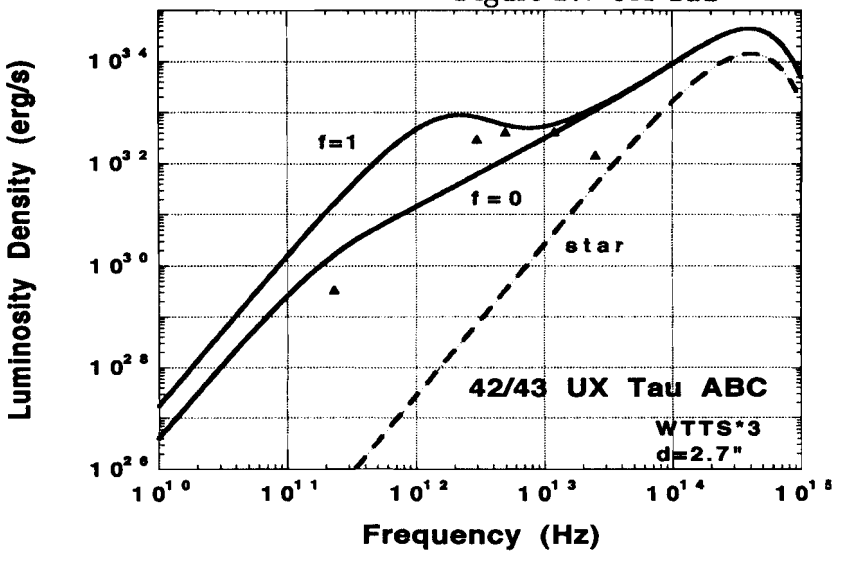

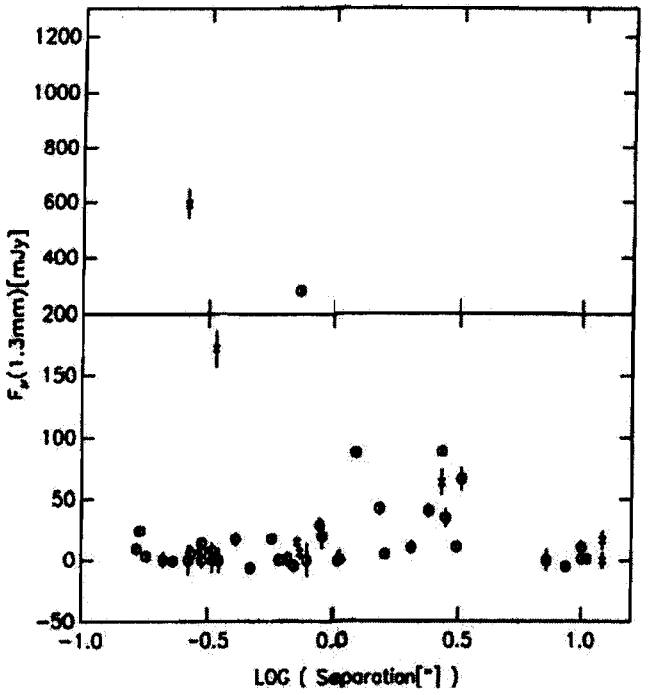

Figure 28: Correlation between binary separations and fluxes

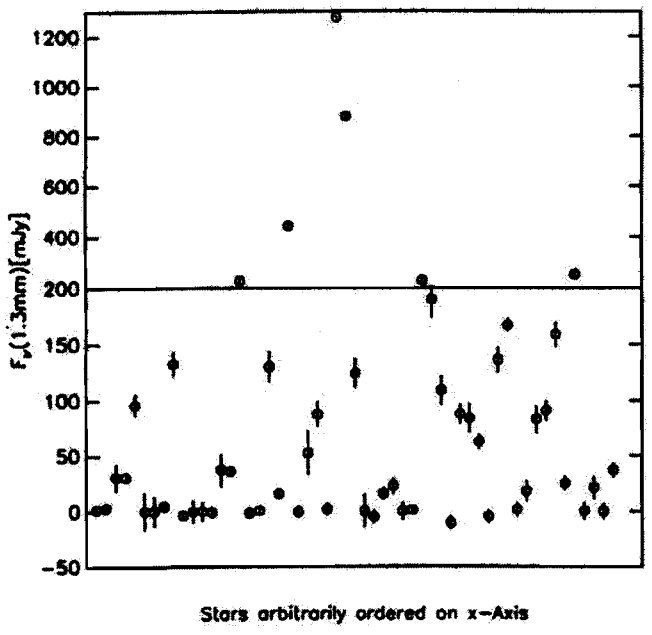

Figure 29: Variation of single star fluxes

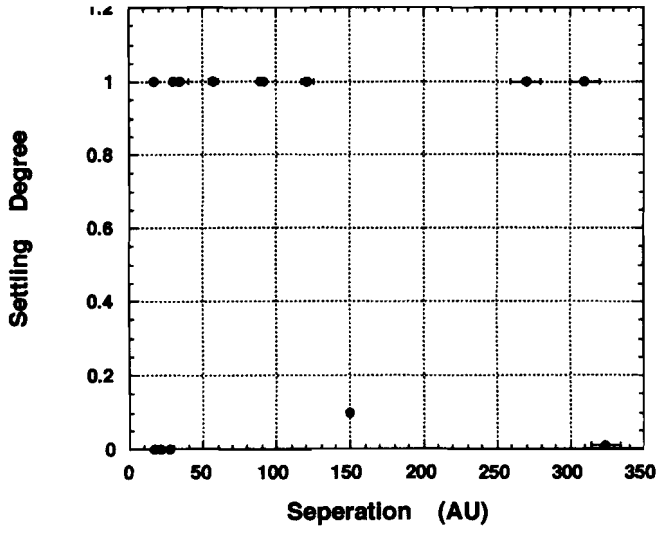

Figure 30: Correlation between binary separations and f-factors

5 Conclusions and discussions

It has been known for almost three decades that the majority of stars are in binary or multiple systems (Heintz 1969 [43]; Batten 1973 [44]). But it is only recently that the question of binary formation has met with substantial interest (Boss 1988 [45]; Bonnell et al. 1991 [46]; Clarke & Pringle 1991a, b [48]; Mouschovias 1991 [49]; Zinnecker 1991 [50]; Chapman et al. 1992 [51]). Through the survey of 104 sample systems in Taurus star forming region, Leinert et al. (1993) [31] shows degree of multiplicity for young stars is higher than for main sequence solar type field stars for the same interval of separation (Duquennoy & Mayor 1991 [52]) by a factor of 1.9 ± 0.3. So, our work might shed light to some unresolved issues of disks around young binaries or multiples.

i) disk formation rate

ii) disk structure (inner hole, flaring, $\cdots$)

iii) difference between close and wide binaries

iv) possibility of planetary system formation

Now we will summarize the conclusions drawn from the previous chapter. First, radiation spectra calculated by our model are well-fitted with the observed fluxes in many sources. This result assures the validity of our passive disk model. Second, as we have already mentioned, closer separation of binaries tends to inhibit dust particle settling. Disks in wide binaries can be treated as a single star because of the smaller effect of companion. In spite of this natural prediction, the result of our calculation shows no significant effect of companion star on the dust particle settling in the disks around binaries. Two main reasons are considered:

1. Not so many binary stars sampled.

2. Observed separations of binaries are *projected separations* and different from physical separations. We even would expect some physically wide binaries to contaminate the close binary sample.

Acknowledgments

First of all, I would like to thank Professor T. Matsuda and Associate Professor Y. Nakagawa for valuable discussions and continuous encouragement. Mr. Hayashi's thourough reading of the manuscript and many suggested corrections were extremely helpful. It is a great pleasure to thank all the members of our laboratory who have been encouraging me and especially Miss Hidaka for helpful support.

Appendix A
Heating and shadowing of a flat thin disk

In this appedix we will discuss the heating and shadowing of a flat thin disk according to the method of Adams & Shu (1986) [14]. Consider the mutual heating and shadowing of two elements of area, dA_* with unit normal $\hat{r}$ on the surface of the star and dA_D with unit normal $\hat{z}$ on the surface of the disk. For purposes of integration over the star when dA_D is held fixed, let the vector position of dA_* expressed in spherical polar coordinates be $\vec{r}_* = (R_*, \theta, \phi)$, and let the vector position of dA_D be $\vec{r}_D = (\omega, \pi/2, 0)$. (We assume here that the disk is perfectly thin and flat; the effects are larger if the disk flares outward or is warped.) For integration over the disk when dA_* is held fixed, it is preferable to ascribe the azimuthal coordinate ϕ to the disk. A light ray from $\vec{r}_*$ to $\vec{r}_D$ has a path vector,

$$s\vec{n} = \vec{r}_D - \vec{r}_*, \tag{11}$$

where s is the path length,

$$s = (R_*^2 + \omega^2 - 2R_*\omega \sin\theta \cos\phi)^{1/2} \tag{12}$$

and $\vec{n}$ is the unit propagation vector with the direction cosines,

$$\vec{n} \cdot \hat{r} = \frac{1}{s}(\vec{r}_D - \vec{r}_*) \cdot \hat{r} = \frac{1}{s}(\omega \sin\theta \cos\phi - R_*), \tag{13}$$

$$\vec{n} \cdot \hat{z} = \frac{1}{s}(\vec{r}_D - \vec{r}_*) \cdot \hat{z} = -\frac{R_*}{s}\cos\theta. \tag{14}$$

If we assume that the disk lies within the opacity gap so that no absorption occurs, the rate, $d\dot{E}_\nu^*$, at which radiant energy of frequency ν traveling from dA_* is intercepted by dA_D, equals

$$d\dot{E}_\nu^* = I_\nu^*(\vec{n} \cdot \hat{r})dA_*(-\vec{n} \cdot \hat{z})dA_D/s^2. \tag{15}$$

We assume that I_ν^* can be approximated as a Planck function $B_\nu[T(\theta)]$. By integrating over all frequencies and over the part of the surface area of the star which can be seen

by dA_D, the radiant energy is intercepted by the upper face of the disk at ω, at a rate per unit area:

$$\frac{d\dot{E}_*}{dA_D} = \frac{1}{\pi}\int_{\theta_\omega}^{\pi/2} \sigma T_*^4(\theta)\sin\theta\cos\theta d\theta \int_{-\phi_\omega}^{+\phi_\omega}\left(\frac{R_*}{s}\right)^4\left(\frac{\omega}{R_*}\sin\theta\cos\phi - 1\right)d\phi. \tag{16}$$

For given θ, the range of the ϕ integration is confined to angles where $\vec{n}\cdot\hat{r} = 0$, i. e., from $-\phi_\omega$ to $+\phi_\omega$ where

$$\cos\phi_\omega \equiv R_*/\omega\sin\theta. \tag{17}$$

The contribution closest to the pole of the star originates at $\theta = \theta_\omega$ with

$$\sin\theta_\omega \equiv R_*/\omega, \tag{18}$$

so that $\phi_\omega = 0$ at this point.

In a steady state, the upper (and lower) side of the disk must radiate not only its own accretion energy, but also the intercepted stellar radiation,

$$\sigma T_D^4(\omega) = \left[\frac{L_D}{4\pi R_*^2(1 - R_*/R_D)}\right]\left(\frac{\omega}{R_*}\right)^{-3} + \frac{d\dot{E}_*}{dA_D}, \tag{19}$$

where L_D represents the total luminosity of the disk. In a similar fashion, the star must radiate not only its own accretion energy, but also the intercepted disk radiation,

$$\sigma T_*^4(\theta) = \frac{1}{2}\rho|v_r|^3 + \eta_*[1 - (1-\eta_D)\mathcal{M}_D][1 - (1-\eta_D)(1-u_*)^{1/2}]\frac{L_0}{8\pi R_*^2} + \frac{d\dot{E}_D}{dA_*}, \tag{20}$$

where $\rho|v_r(R_*,\theta)|^3/2$ is the rate of release of impact energy by direct infall and where we have spread the stellar dissipation of rotational energy in a spherically symmetric manner for lack of better knowledge. If equation (19), the rate of intercepted disk energy is

$$\frac{d\dot{E}_D}{dA_*} = \frac{1}{\pi}\cos\theta\int_{\omega_*}^{R_D}\sigma T_D^4(\omega)\frac{\omega d\omega}{R_*^2}\int_{-\phi_\omega}^{+\phi_\omega}\left(\frac{R_*}{s}\right)^4\left(\frac{\omega}{R_*\sin\theta\cos\phi} - 1\right)d\phi, \tag{21}$$

where

$$\omega_* \equiv R_*/\sin\theta, \tag{22}$$

is the smallest radius of the disk observable at θ on the star.

In principle, equations (19) and (20) should also include the effect of the back warming of a hot dust envelope. If the infalling envelope is optically thick near the dust destruction front, heating by the infalling dust envelope effectively adds the terms $\gamma_*(\omega)\sigma T_d^4$ and $\gamma_D(\theta)\sigma T_d^4$, respectively, to the right-hand sides of equations (19) and (20), where $\gamma_*(\omega)$ is the fraction of the sky viewed from ω in the disk not blocked by the star and $\eta_D(\theta)$ is the fraction of the sky viewed from θ on the star not blocked by the disk. In practice, as long as T_*^4 and T_D^4 remain large in comparison with T_d^4, the correction is a minor effect.

Equations (19) and (20), together with the subsidiary definitions (16) and (21), constitute two coupled integral equations which determine $T_D(\omega)$ and $T_*(\theta)$. For the purposes of this appendix, it suffices to find an approximate global solution to the set. We assume $T_*(\theta) = \text{constant} \equiv T_*$ and $T_D(\omega) = T_{D^*}(\omega/R_*)^{-3/4}$, and we choose the constants T_* and T_{D^*} such that equations (19) and (20) are valid when integrated over the *entire* surfaces of disk and star. The integrations with respect to dA_D and dA_* produce two requirements:

$$4\pi R_*^2 \left(1 - \frac{R_*}{R_D}\right) \sigma T_{D^*}^4 = L_D + \dot{E}_*, \tag{23}$$

$$4\pi R_*^2 \sigma T_*^4 = L_* + \dot{E}_D, \tag{24}$$

and

$$\dot{E}_* = 8\pi R_*^2 \sigma T_*^4 \int_{R_*}^{R_D} \frac{\omega d\omega}{R_*^2} \int_{\theta_\omega}^{\pi/2} \sin\theta\cos\theta d\theta \int_0^{\phi_\omega} \left(\frac{R_*}{s}\right)^4 \left(\frac{\omega}{R_*}\sin\theta\cos\phi - 1\right) d\phi, \tag{25}$$

$$\begin{aligned} \dot{E}_D &= 8\pi R_*^2 \sigma T_{D^*}^4 \int_{\theta_{*D}}^{\pi/2} \sin\theta\cos\theta d\theta \int_{\omega_*}^{R_D} \left(\frac{\omega}{R_*}\right)^{-3} \frac{\omega d\omega}{R_*^2} \\ &\times \int_0^{\phi_\omega} \left(\frac{R_*}{s}\right)^4 \left(\frac{\omega}{R_*}\sin\theta\cos\phi - 1\right) d\phi, \end{aligned} \tag{26}$$

with

$$\sin\theta_{*D} \equiv R_*/R_D. \tag{27}$$

We can write equations (25) and (26) in the suggestive forms:

$$\dot{E}_* = f_D 4\pi R_*^2 \left(1 - \frac{R_*}{R_D}\right) \sigma T_*^4, \tag{28}$$

$$\dot{E}_D = f_* 4\pi R_*^2 \sigma T_{D^*}^4, \tag{29}$$

where by introducing the transformation of variables:

$$u \equiv R_*/\omega,\ v \equiv \sin\theta,\ w \equiv \cos\phi, \tag{30}$$

and by switching one order of integration, we may express f_D and f_* as the dimensionless integrals:

$$\begin{aligned} f_D &= \frac{2}{\pi(1-u_{*D})}\int_{u_{*D}}^1 h(u)du, \\ f_* &= \frac{2}{\pi}\int_{u_{*D}}^1 u^3 h(u)du, \end{aligned} \tag{31}$$

$$h(u) \equiv \int_u^1 vdv \int_{u/v}^1 \frac{(vw-u)dw}{(1-w^2)^{1/2}(1+u^2-2uvw)^2}, \tag{32}$$

with $u_{*D} \equiv R_*/R_D$. By a judicious change of variables (motivated by switching to a spherical coordinate system the line joining the center of the star and the disk point becomes the polar axis), we can integrate equation (32) to obtain

$$h(u) = \frac{1}{2u}[\arcsin u - u(1-u^2)^{1/2}]. \tag{33}$$

The substituition of equation (33) into equations (31) now yields

$$f_D = \frac{1}{(1-u_{*D})}\left[\frac{1}{4} - \frac{1}{\pi}\left(1-\frac{1}{2u_{*D}^2}\right)\arcsin u_{*D} - \frac{1}{2\pi u_{*D}}(1-u_{*D}^2)^{1/2}\right], \tag{34}$$

$$f_* = \frac{1}{2} - \frac{u_{*D}}{\pi}\arcsin u_{*D} - \frac{1}{3\pi}(1-u_{*D}^2)^{1/2}(4-u_{*D}^2). \tag{35}$$

The functions f_D and f_* are shown in Table 3 of Adams & Shu (1986) [14]; of special interest are the limiting values, $f_D = 1/4$ and $f_* = 1/2 - 4/3\pi = 0.0756$ for $u_{*D} = 0$. Note also that $f_D = 1/2$ for $u_{*D} = 1$ because half of the sky is filled with the stellar surface for a nallow disk at the equator of the star.

With equations (28) and (29) giving $\dot{E}_*$ and $\dot{E}_D$, we may solve equations (23) and (24) as a set of simultaneous linear equations for σT_*^4 and $\sigma T_{D^*}^4$, obtaining

$$\sigma T_*^4 = \frac{1}{(1-f_* f_D)}\left[\frac{L_*}{4\pi R_*^2} + f_* \frac{L_D}{4\pi R_*^2(1-u_{*D})}\right], \tag{36}$$

$$\sigma T_{D^*}^4 = \frac{1}{(1-f_* f_D)}\left[\frac{L_D}{4\pi R_*^2(1-u_{*D})} + f_D \frac{L_*}{4\pi R_*^2}\right]. \tag{37}$$

Appendix B
Reprocessing of protostellar radiation in a flared disk

In this appendix we give a short discussion of the protostellar radiant flux absorbed by the surface of a flared accretion disk according to the method of Ruden & Pollack (1991) [12]. The special case where the disk is considered to be razor thin ($H = 0$) has been considered by Friedjung (1985) [13] and Adams & Shu (1986) [14] as we have described in appendix A. The general case where the disk height is nonzero has been discussed by Kenyon & Hartmann (1987) [53], but their discussion in an appendix of their paper contains some misprints. In the following, we apply the general method presented in the appendix of Adams & Shu (1986) [14].

Let the center of the disk be in the $z = 0$ plane, and denote the distance from z-axis by ω. The surface of the disk is a distance $H(\omega)$ above the midplane, so that the spherical radius r satisfies $r^2 = \omega^2 + H^2$. Let $\hat{n}_d$ be the normal to the surface element dA_* on the stellar surface, and $\hat{s} = s\hat{n}$ be the ray from the element dA_* to the disk surface. The energy flux from dA_* that is intercepted normally by unit area of the disk surface is

$$F_\nu = B_\nu(T_*) \int\int_{A_*} \frac{dA_*}{s^2} (\hat{n} \cdot \hat{n}_*)(-\hat{n} \cdot \hat{n}_d), \tag{38}$$

where we assume that the star radiates like a blackbody with a constant surface temperature T_*. To evaluate the surface integral, it proves most convenient to use a spherical coordinate system where the polar axis is along the line joining the center of the star and a disk surface element. With respect to this axis, the polar angle is ψ and the azimuthal angle is ϕ. In this coordinate system, the integral for the total stellar flux intercepted by the disk becomes

$$\begin{aligned} F_d &= 2 \int_0^\infty B_\nu(T_*) \int_0^{\psi_{max}} \sin\psi d\psi \\ &\times \int_0^{+\phi_{max}} d\phi [\cos\psi \sin(\alpha - \beta) + \sin\psi \cos\phi \cos(\alpha - \beta)], \end{aligned} \tag{39}$$

where the following angles have been defined:

$$\tan\alpha = \frac{dH}{d\omega}, \ \tan\beta = \frac{H}{\omega}, \ \sin\psi_{max} = \frac{R_*}{r}, \tag{40}$$

and where ϕ_{max} is a complicated function of ψ and r whose specific form is not needed. Equation (39) is equivalent to equation (A4) of Kenyon & Hartmann (1987) [53] if their ratios c_1/c_3 and c_2/c_3 are identified as $\cos(\alpha - \beta)$ and $\sin(\alpha - \beta)$, respectively. It is also equivalent to the formulae derived by Friedjung (1985) [13] and Adams & Shu (1986) [14] if $H = 0$ (i.e., $\alpha = \beta$) and $\phi_{max} = \pi/2$. It is evident from equation (39) that unless α is greater than or equal to β, the inclination of the disk surface (with respect to $\hat{z}$) is too small for direct solar illumination to fall normally on the disk at radius ω. Futhermore, if $\beta(\omega)$ is not a monotonically increasing function of ω, then the inner disk regions will shadow some or all of the outer disk regions from direct illumination by the central star.

In this paper, we focus our attention primarily on the disk regions that are relatively far from the star, $\omega \gg R_*$, and that are geometrically thin, $H \ll \omega$. In this regime, it can be shown that the approximation $\phi_{max} = \pi/2$ is valid, a result which is exact in the limit $H \to 0$. The physical content of using this approximation is that when $H \ll \omega$, the primary effect of disk flaring on the amount of intercepted stellar flux is due to the *tilt* of the disk surface toward the star rather than due to the height of the disk surface above the midplane $z = 0$. Using $\phi_m = \pi/2$, equation (39) can be integrated analytically to yield

$$F_d = \sigma T_*^4 \left[\frac{1}{2} \sin(\alpha - \beta) \sin^2 \psi_{max} + \frac{1}{\pi} \cos(\alpha - \beta)(\psi_{max} - \sin \psi_{max} \cos \psi_{max}) \right]. \quad (41)$$

In the limit that $H \ll \omega$ and $\omega \gg R_*$, we can manipulate this equation into the form

$$F_d = \sigma T_*^4 \left[\frac{2}{3\pi} \left(\frac{R_*}{\omega} \right)^3 + \frac{1}{2} \left(\frac{R_*}{\omega} \right)^2 \left(\frac{H}{\omega} \right) \left(\frac{d \ln H}{d \ln \omega} - 1 \right) \right]. \quad (42)$$

The first term on the right-hand side is the same as derived by Friedjung (1985) [13] and Adams & Shu (1986) [14] for a flat disk $H = 0$. The second term in the right-hand side is a correction due to disk flaring, which is only nonzero if $d \ln H / d \ln \omega > 1$, that is if $\alpha > \beta$. The second term dominates the disk surface flux when $H(\omega) \gg R_*$, which is true in the planet formation regions of the solar nebula. Equation (42) was first stated (without derivation) by Kusaka, Nakano, & Hayashi (1970) [11]. We can derive the temperature distribution of the disk from equation (42) by defining the disk surface

temperature to be $T(r) \equiv (F_d/\sigma)^{1/4}$ and by rewriting ω in the more conventional notation as r (from which it differs only by terms of second order in H/ω) in the following,

$$T(r) = T_* \left[\frac{2}{3\pi} \left(\frac{R_*}{r} \right)^3 + \frac{1}{2} \left(\frac{R_*}{r} \right)^2 \left(\frac{H}{r} \right) \left(\frac{d \ln H}{d \ln r} - 1 \right) \right]^{1/4}. \tag{43}$$

Assuming a Planck distribution at the stellar surface: $L_* = 4\pi R_*^2 \sigma T_*^4$, we can obtain the first two terms of equation (5) in section 2.2.

Appendix C
Viscous heating by mass accretion inside a disk

In this appendix we describe the viscous heating caused by turbulent motion inside the disk according to the method performed by Shakura & Sunyaev (1973) [16]. Their derivation is based on the disk mass accretion to black holes, but their method can be applied to our disk model.

To a first approximation, the disk materials may be assumed to rotate around a central star in circular Keplerian orbits

$$v_K = \sqrt{\frac{GM_*}{r}},\ \Omega_K = \sqrt{\frac{GM_*}{r^3}}. \tag{44}$$

The friction between adjacent layers, connected with the existence in the disk of turbulence and chaotic, small scale magnetic fields, leads to the loss of the angular momentum of the particles. A radial component of velocity appears and the particles spiral inward to the central star

$$\frac{\Sigma_0 d\Omega_K r^2}{dt} = -\Sigma_0 v_r \frac{d\Omega_K r^2}{dr} = \frac{1}{r}\frac{d}{dr} W_{r\phi} r^2. \tag{45}$$

Here, $\Sigma_0 = 2\int_0^{z_0} \rho dz$ is the surface density of matter in the disk, $W_{r\phi}$ is the stress between the adjacent layers. In scales comparable with the radius r, turbulence is homogeneous and isotropic. To describe the average motions in the presence of such turbulence one may use the formulae obtained for laminar flows on replacing the molecular viscosity by the turbulent one $\eta_t = \rho v_t l$. Here, η_t, v_t, and l are the turbulent viscosity, the turbulent velocity, and the maximal scale of the turbulent cell, respectively. For tangential stresses, we have

$$w_{r\phi} = \eta_t R_d \frac{d\Omega_K}{dr} \sim -\eta_t \frac{v_K}{r} \sim -\rho c_s^2 \frac{v_t}{c_s} \tag{46}$$

where the disk thickness $z_0 \sim r c_s / v_K$. Thus the efficiency of two of the most important mechanisms of angular momentum transport connected with the magnetic field (which always is present in astrophysical conditions) and turbulence (whose existence in the disk is less definite)

$$-w_{r\phi} \sim \rho c_s^2 \frac{v_t}{c_s} + \rho v_s^2 \frac{H^2}{4\pi \rho c_s^2} = \alpha \rho c_s^2 \tag{47}$$

can be characterized by only one parameter, α. According to equation (47)

$$W_{r\phi} = 2\int_0^{z_0} w_{r\phi} dz = -\alpha \Sigma_0 c_s^2. \tag{48}$$

In stationary conditions, $v_r < 0$ and $\dot{M} = 2\pi\Sigma_0 v_r r = \text{const}$ and integrating equation (45) we obtain

$$\dot{M}\Omega_K r^2 = -2\pi W_{r\phi} r^2 + C. \tag{49}$$

Practically the whole angular momentum is transported outward and only a small fraction of the initial angular momentum falls together with matter into the central star. The constant in equation (49) is determined by the condition, $W_{r\phi} \simeq 0$ on the last stable orbit. A self-consistent axialsymmetric picture uses injection of matter at some R_1. Part of matter situated at R_1 falls on the star but one must imagine also matter flows beyond R_1, taking away the excess of an angular momentum.

In a direction perpendicular to the plane of the disk the normal component of the gravitational force of the star is balanced by the sum of the pressure gradients of gas, radiation turbulent and magnetic pressures. The equation of hydrodynamic equiribrium gives the half thickness of the disk

$$z_0 = \frac{c_s}{v_K} r. \tag{50}$$

In losing their angular momentum the particles also lose their gravitational energy. Part of the latter goes to increasing the kinetic energy of rotation and the other part is converted into thermal energy and can be radiated from the surface of the disk. The forces leading to the angular momentum transfer in a rotating system also induce the energy flow equal to $-2\pi W_{r\phi} r^2 \Omega_K$. In Keplerian motion with Ω_K increasing inward and $W_{r\phi} < 0$, the energy flow is directed outward. The rate of the energy dissipation in the ring between R_2 and R_3 has a term equal to divergence of this energy flow. Collecting all terms, one obtains the energy flux, radiated from unit surface of the disk in unit time

$$\begin{aligned} Q &= \frac{1}{2} W_{r\phi} r \frac{d\Omega_K}{dr} \\ &= \frac{1}{4\pi r}\frac{d}{dr}\left[\dot{M}\left(\frac{v_K^2}{2} - \frac{GM_*}{r}\right) - 2\pi r^2 W_{r\phi}\Omega_K\right] \end{aligned}$$

$$= \frac{3}{8\pi}\frac{GM_*\dot{M}}{r^3}\left(1-\sqrt{\frac{R_*}{r}}\right). \tag{51}$$

This is equivalent to the last term of equation (5) in section 2.2 of our thesis.

References

[1] Hayashi, C., Nakazawa, K., & Nakagawa, Y., "Formation of the Solar System", Protostars and Planets II, 1100 (1985)

[2] Jeans, J. H., The configurations of rotating liquid masses. In Astronomy and Cosmology, Cambridge University Press (1929).

[3] Sekiya, M., poster presentation at autumn session of Japanese Astronomical Society in 1997

[4] Safronov, V. S., "Evolution of the Protoplanetary Cloud and Formation of the Earth and Planets", (Moscow: Nauka Press) (1969); also NASA TTF-677 (1972)

[5] Adams, F. C., Emerson, J. P., & Fuller, G. A., Ap. J., **357**, 606 (1990)

[6] Adams, F. C., Lada, C. J., & Shu, F. H., Ap. J., **326**, 865 (1988)

[7] Osterloh, M. & Beckwith, S. V. W., Ap. J., **439**, 288 (1995)

[8] Hayashi, C., Prog. Theor. Phys. Suppl., **70**, 35 (1981)

[9] Beckwith, S. V. W., & Sargent, A. I., Ap. J., **381**, 250 (1991)

[10] Miyake, K., & Nakagawa, Y., Ap. J., **441**, 361 (1995)

[11] Kusaka, T., Nakano, T, & Hayashi, C., Prog. Theor. Phys., **44**, 1580 (1970)

[12] Ruden, S. P., & Pollack, J. B., Ap. J., **375**, 740 (1991)

[13] Friedjung, M., A&A, **146**, 366 (1985)

[14] Adams, F. C., & Shu, F.H., Ap. J., **308**, 836 (1986)

[15] Lynden-Bell, D., & Pringle, J. E., MNRAS, **168**, 603 (1974)

[16] Shakura, N. I. & Sunyaev, R. A., A&A, **24**, 337 (1973)

[17] Chiang, E. I. & Goldreich, P., Ap. J., **490**, 368 (1997)

[18] Draine, B. T., & Lee, H. M., Ap. J., **285**, 89 (1984)

[19] Miyake, K., & Nakagawa, Y., ICARUS, **106**, 20 (1993)

[20] Weidenschilling, S. J., ICARUS, **44**, 172 (1980)

[21] Nakagawa, Y., Nakazawa, K., & Hayashi, C., ICARUS, **45**, 517 (1981)

[22] Nakagawa, Y., Sekiya, M., & Hayashi, C., ICARUS, **67**, 365 (1986)

[23] Beckwith, S. V. W., & Sargent, A. I., Chini, R. S., & Gusten, R., AJ., **99**, 924 (1990)

[24] Rucinski, S. M., AJ., **90**, 2321 (1985)

[25] Mundt, R., Walter, F. M., Feigelson, E. D., Finkenzeller, U., Herbig, G. H., Odell, A. P., Ap. J., **269**, 229 (1983)

[26] Reipurth, B., Lindgren, H., Nordstrom, B., Mayor, M., A& A, **235**, 197 (1990)

[27] Herbig, G. H., & Bell, K. R., Lick Obs., Bull., 1111 (1988)

[28] Gomez, M., Jones, B. F., Hartmann, L., Kenyon, S. J., Stauffer, J. R., & Reid, I. N., AJ., **104**, 762 (1992)

[29] Hartmann, L., Jones, B. F., Stauffer, J. R., & Kenyon, S. J., AJ., **101**, 1050 (1991)

[30] Jones, B. F., & Herbig, G. H., AJ., **84**, 1872 (1979)

[31] Leinert, C. H., Zinnecker, H., Weitzel, N., Christou, J., Ridgway, S. T., Jameson, R., Haas, M., & Lenzen, R., A&A, **278**, 129 (1993)

[32] Walter, F. M., Brown, A., Mathieu, R. D., Myers, P. C., & Vrba, F. J., AJ., **96**, 297 (1988)

[33] Herbig, G. H., Ap. JS, **4**, 337 (1960)

[34] Herbig, G. H., Ap. J, **217**, 693 (1977)

[35] Weaver, W. M. B., & Jones, G., Ap. JS, **78**, 239 (1992)

[36] Thum, C., et al., IRAM Working Report, 212 (1992)

[37] Elias, J. H., Ap. J., **224**, 857 (1978)

[38] Hartigen, P., Kenyon, S. J., Hartmenn, L., Strom, S. E., Edwards, S., Welty, A. D., & Stauffer, J., Ap. J., **382**, 617 (1991)

[39] Cardelli, J. A., Clayton, G. C., & Mathis, J. S., Ap. J., **345**, 245 (1989)

[40] Cohen, M. & Kuhi, L. V., Ap. JS, **41**, 743 (1979)

[41] Strom, S. E., Strom, K. M., Edwards, S., Cabrit, S., & Skrutskie, M. F., AJ., **97**, 1451 (1989)

[42] Natta, A., Ap. J., **412**, 761 (1993)

[43] Heintz, W. D., J. R. Astron. Soc. Can. **63**, 275 (1969)

[44] Batten, A. H., Binary and Multiple Systems of Stars, Pergamon Press, New York (1973)

[45] Boss, A. P., Comments Ap., **12**, 169 (1988)

[46] Bonnell, I., Martel, H., Bastien, P., Arcoragi, J. P., Benz, W., Ap. J., **377**, 553 (1991)

[47] Boss, A. P., Nature, **351**, 298 (1991)

[48] Clarke, C. J., Pringle, J., MNRAS, **249**, 584 (1991a); Clarke, C. J., Pringle, J., MNRAS, **249**, 588 (1991b)

[49] Mouschovias, T., Ap. J., **373**, 169 (1991)

[50] Zinnecker, H., in: "Fragmentation of Molecular Clouds", Eds. Falgarone et al., IAU Symposium 147, p.526 (1991)

[51] Chapman, S., Pongracic, H., Disney, M., Nelson, A., Turner, J., Whiteworth, A., Nature, **359**, 207 (1992)

[52] Duquennoy, A., & Mayor, M., A&A, **248**, 455 (1991)

[53] Kenyon, S. J., & Hartmann, L.W., Ap. J., **323**, 714 (1987)